Research Article

Yuanjie Huang*

Tangential electrostatic field at metal surfaces

https://doi.org/10.1515/phys-2022-0270
received February 09, 2023; accepted June 24, 2023

Abstract: In electrodynamics, it has been long believed that when the electrostatic equilibrium is reached the electrostatic field outside a metal is always perpendicular to the metal surface. However, the tangential electrostatic field (TEF) may be discovered at the metal surface through the mechanical-electric coupling in the work. The TEF can lead to new knowledge and more accurate modification on electrostatics of metals including the electrostatic equilibrium conditions, uniqueness theorem, method of image charges, electrostatic shielding, Thompson's theorem, and Green's reciprocation theorem. The TEF and the mechanical-electric coupling can also indicate that an intrinsically intensive electrostatic field may exist at the nanoparticle surface. Thereby a unified model could be constructed for the surface-enhanced Raman scattering (SERS) which has been a long-standing problem in physics and chemistry in recent several decades. Furthermore, when the micro-electro-mechanical systems (MEMS) work, the deformation of the metal plate can induce an additional electrostatic field and a newly attractive electrostatic force between the metal plates. They may be important for the design and fabrication of high-performance MEMS devices. Overall, the revealed TEF may update the physical knowledge of the electrostatics of metals in electrodynamics and may acquire widespread applications in the areas of SERS, MEMS, and so on.

Keywords: electrodynamics, electrostatic equilibrium conditions, tangential electrostatic field, electron chemical potential, surface-enhanced Raman scattering, micro-electro-mechanical systems

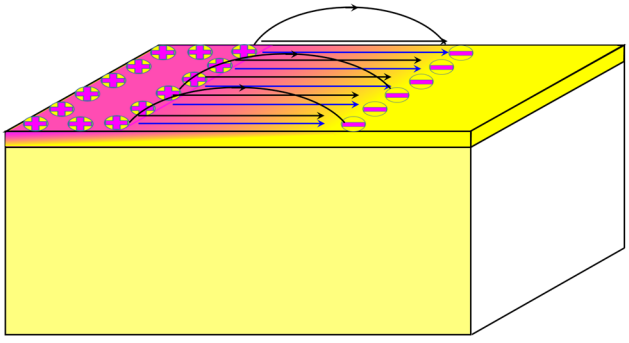

Graphical abstract

1 Introduction

In the classical electrodynamics, it has been long believed that when the electrostatic equilibrium is reached, the electrostatic field inside a metal is rigorously zero so that the metal is an equipotential body and there is no net electric charges inside the metal [1–4]. The electrostatic equilibrium for a metal requires that the electrical current is zero in the metal. Hence, the electric field in the metal must be zero according to the famous Ohm's law [1–4]. Otherwise, any remnant electric field would push the free electrons to move, forming an electrical current in the metal [1–4], which violates against the electrostatic equilibrium. In another respect, the classical electrostatic theory also shows that the electrostatic field must be perpendicular to the metal surfaces and there is no tangential component along the metal surfaces [1–4]. If there was a tangential component, no matter how weak it would be, the free electrons would move along the metal surface and an electrical current would emerge [1–4], as is forbidden by the electrostatic equilibrium as well. To one's surprise, the carefully performed experiments found that the surface electric potential usually displays variations of a few millivolts at the metal surfaces [5–7], and the surface potential variations at the metal surfaces are sometimes referred to as Patch effect [7,8]. The important experimental results may enlighten people that the tangential electrostatic field (TEF) might be allowed along the metal surfaces. However, it is completely contradictory to the traditional belief in the electrostatics of metals and has been a puzzling topic in recent years.

To address the puzzling topic and explain the observed surface potential variations at the metal surfaces, the presence of TEF along the metal surfaces may be proved and uncovered theoretically in the work. The related proof is given in Section 2. According to the TEF and the electrostatic field inside a metal, the traditional electrostatics of

* **Corresponding author: Yuanjie Huang**, National Interdisciplinary Research Center (To be established), China Academy of Engineering Physics, Mianyang 621900, China, e-mail: hyj201207@163.com

metals is reexamined and investigated in Section 2.1. The related interesting physical effects is subsequently studied in some fields in Section 2.2. At last, the conclusions are summarized in Section 3.

2 Results and discussion

In electrostatics of metals, the key question is "Does any electric field inevitably cause an electrical current in a metal?" By means of investigation, it was found that an electric field cannot always cause an electrical current in a metal and sometimes the electrical current could be zero even if there exists a strong electrostatic field in the metal. This point was revealed and gave birth to a new discovery of a mechanical-electric coupling in metals, *i.e.*, Yuheng Zhang effect [9]. This effect can point out that any actual metal at electrostatic equilibrium may no longer be an equipotential body and there may always exist an electric field inside the metal considering the widespread dislocations and various strains [9–11]. At electrostatic equilibrium, the electrostatic field inside the metals may be given by Yuheng Zhang equation [9,10] as follows:

$$\nabla E_{\mathrm{F}}(\vec{r}) = e\vec{E}, \tag{1}$$

where e is the electron (positron) charge, $\vec{E}$ is the electrostatic field, and E_{F} is the position-dependent electron (positron) chemical potential and sometimes it is known as Fermi level (not Fermi energy). As is known, the chemical potential of a particle system was introduced by Gibbs in 1876 [12]. It may be appropriate for the system with the particle number conservation. In general, if the charged particles possess a volume, the related chemical potential usually includes the contributions of the carried electric dipole, electric quadrupole, and so on. But for the point particles without volume, there may be no electric dipole and higher order electric moments, so the corresponding chemical potential may be only relevant to the carried net charge. Therefore, Yuheng Zhang equation may rigorously hold right for electron (positron) systems satisfying the following requirements: (i) the electron (positron) systems must be in an equilibrium state; (ii) the electron (positron) system must conform to the number conservation; and (iii) the electron (positron) must be a point particle and does not exhibit any measurable volume effect, which is an important foundation for the quantum electrodynamics. Yuheng Zhang equation might be a fundamental physical relation, and could not be derived by quantum mechanics, because the point particle assumption for electrons (positrons) may not be addressed by the quantum mechanics. In this equation, the electron chemical potential may exhibit the statistical properties of studied electron (positron) systems and it usually depends on the quantum properties of the electron (positron) systems. As a result, Yuheng Zhang equation may statistically contain the quantum characteristics of electron (positron) systems no matter how complex their interaction and the experienced fields could be. The equation may find important applications in some fields. For example, the unraveled existence of the electrostatic field inside metals may induce some interesting physical effects which were previously addressed [9,10].

Enlightened by Yuheng Zhang effect [9], the electrostatic equilibrium requires the zero electrical current in metals but could permit existence of electrostatic field. Likewise, at the metal surfaces, the electrostatic equilibrium forbids any electrical current along the metal surfaces but could allow the TEF, meaning that the TEF could exist if it cannot generate an electrical current.

Even for single-crystalline metals, there still exist many factors such as residual stresses [13,14], various defects [15], surface reconstruction, surface tension, and chemical adsorption, which may alter the Fermi level E_{F}, *i.e.*, electron chemical potential. As a result, the free electrons in the metal may move from the higher Fermi level regions to lower Fermi level regions. The transfer of electrons would produce an electrical current and also cause an electric field between the higher Fermi level regions and lower Fermi level regions based on Gauss' law. The generated electrical current may be written as follows [16,17]:

$$\vec{J} = \sigma(0)\vec{E} - \frac{\sigma(0)}{e}\nabla E_{\mathrm{F}}, \tag{2}$$

where J is the electrical current density, and $\sigma(0)$ is the direct current electric conductivity of the metal. In this equation, the first term on the right denotes the electrical current generated by the electric field, whereas the second term originates from the directional electron transfer induced by the alteration of Fermi level. When the electrostatic equilibrium is approached, one may substitute Yuheng Zhang equation in the above equation and find that the electric current is indeed zero, as is the requirement of the electrostatic equilibrium. As a result, an electrostatic field is generated between the higher Fermi level regions and lower Fermi level regions in the metal. The electron transfer usually affects Fermi level of low-dimensional materials, so the position dependence of Fermi level in Eqs. (1) and (2) should take the values which have taken electron transfer effect on Fermi level into account at electrostatic equilibrium.

According to Eqs. (1) and (2), the null electrical current at electrostatic equilibrium could allow the presence of a

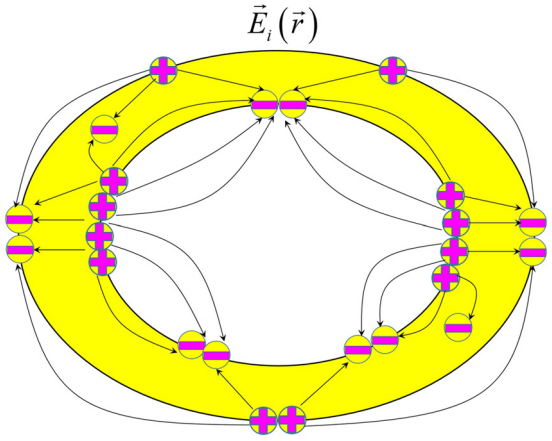

Figure 1: Distribution of the intrinsic electrostatic field and the related electric charges in a closed metal shell. The plus circles and the minus circles present the positive charges and negative charges, respectively. The black arrows denote the intrinsic electrostatic field inside the metal and outside the metal.

non-null macroscopic intrinsic electrostatic field (denoted by $E_i(r)$) inside a metal shown in Figure 1 and it is as follows:

$$\vec{E}_i(\vec{r}) = \nabla E_F(\vec{r})/e. \tag{3}$$

The related intrinsic electrostatic potential for the metal can be obtained as follows:

$$\varphi_i(\vec{r}) = -\frac{E_F(\vec{r})}{e} + \frac{\mu_e}{e}, \tag{4}$$

where $\varphi_i(r)$ stands for the unique and intrinsic electrostatic potential of a metal and it fulfills the relation $E_i(r) = -\nabla\varphi_i(r)$, and μ_e is the electrochemical potential of the electrons. This indicates that any metal at an electrostatic equilibrium is an equal-electrochemical potential body but not an equipotential body. Only when the Fermi level of a metal is a constant and cannot exhibit position dependence (this type of metal does not exist in real life), may the metal be an equipotential body where both the electrostatic field inside the metal and the TEF at the metal surface is zero.

Similarly, in the case of metal surface at electrostatic equilibrium, Eqs. (1) and (2) reveal that the zero electrical current at the metal surface permits a non-null intrinsic TEF (denoted by $E_{it}(r)$) which may arise from the position dependent Fermi level at the metal surface. These conclusions may also be valid for a perfect conductor where a large number of freely moving electrons exist and the direct current electrical conductivity approaches infinity, *i.e.*, $\sigma(0) \to \infty$. Therefore, the electrostatic field may not always be normal to the metal surfaces, but a TEF resulting from the lift of Fermi level may appear along metal surfaces, as is illustrated in Figure 2. The existence of TEF may

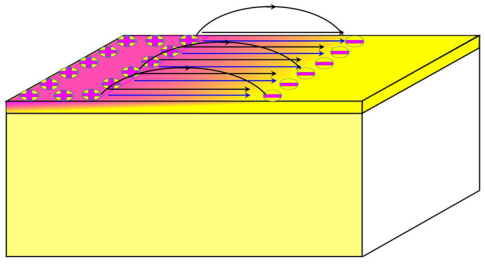

Figure 2: Schematic diagram of the TEF at metal surfaces. Magenta regions denote the metal surface with higher Fermi level, while yellow regions show the lower Fermi level regions. Positive and negative signs represent positive and negative charges, respectively. Blue arrows stand for the TEF at the metal surfaces and the black ones denote the field outside the metal surface.

agree with the carefully performed experiments which uncovered the surface potential variations of a few millivolts at metal surfaces [5–7].

The existence of the intrinsic electrostatic field $E_i(r)$ inside the metal and the TEF $E_{it}(r)$ at the metal surface not only can generate new understandings of the electrostatics of metals but also can give birth to interesting physical effects, which are addressed in the following sections.

2.1 New understandings of electrostatics of metals

2.1.1 Electrostatic equilibrium conditions (EECs) for metals

For a metal placed in a complex electrostatic environment, the surrounding charges and electric field may exert an external electrostatic potential on the metal. The application of the external potential does not usually influence the Fermi level and the intrinsic electrostatic potential $\varphi_i(r)$ of the metal. Considering the intrinsic potential $\varphi_i(r)$ and the external potential, the total electrostatic potential of the metal may be written as the following equation, which is a result of the superposition principle for the electric fields and electrostatic potentials [18–20]:

$$\varphi(r) = \varphi_i(r) + \varphi_e(r), \tag{5}$$

where $\varphi(r)$ is the total electrostatic potential for the metal and it is usually position dependent, and $\varphi_e(r)$ denotes the external electrostatic potential including the contribution from the induction charges at the metal surface. Correspondingly, the electrostatic field inside the metal may be given as follows:

$$E(r) = E_i(r) + E_e(r), \tag{6}$$

where $E(r)$ is the total electrostatic field in the metal and it is given by $E(r) = -\nabla\varphi(r)$, $E_i(r)$ is the intrinsic electrostatic field and it is given by $E_i(r) = -\nabla\varphi_i(r)$, $E_e(r)$ is the electrostatic field induced by the external potential and it is given by $E_e(r) = -\nabla\varphi_e(r)$. Upon reaching the electrostatic equilibrium, very interestingly, the external electrostatic potential $\varphi_e(r)$ is position independent and is a constant for the whole metal according to Yuheng Zhang equation. So, it may be concluded that a metal is an equipotential body where the "potential" refers to the external electrostatic potential. In other words, the electrostatic field $E_e(r)$ induced by any external electrostatic potential $\varphi_e(r)$ is always zero inside the metal, *i.e.*,

$$E_e(r) = 0. \tag{7}$$

Meanwhile, the external potential-induced electrostatic field at the metal surface must be normal to the surface and the related TEF must be zero at the metal surface,

$$E_{et}(r) = 0, \tag{8}$$

where $E_{et}(r)$ stands for the TEF component of $E_e(r)$ at the metal surface. Thus, the traditional EEC for a metal should be modified and summarized as follows:

1) A metal cannot be an equipotential body, but it must be an "equipotential" body where the "equipotential" refers to the external electrostatic potential containing the contribution of induction charges at the metal surfaces.
2) Inside a metal, an intrinsic electrostatic field always exists, but the electrostatic field generated by any external electrostatic potential must be zero.
3) An intrinsic TEF is popular at the metal surface, but the TEF originating from any external electrostatic potential must be zero at the metal surfaces.
4) The intrinsic net charges due to the intrinsic electrostatic field can exist inside a metal, but the externally charged or discharged charges cannot reside inside the metal and must be distributed at the metal surfaces.

In the above statements on the modified electrostatic equilibrium conditions (MEEC), a metal refers to any real single-component metal or multi-component alloy which contains many "freely" moving electrons and exhibits a large electrical conductivity. Different from definitions in many textbooks [4,18–20], it does not require a uniform composition and an infinite electrical conductivity. The MEEC may be appropriate under the conditions that the state of the metal, *e.g.*, stress distribution, the number and distribution of various defects, and composition distribution, keeps invariant on the application of external electrostatic potential. Nevertheless, in some extreme cases, the externally applied electrostatic potential can change the state and indirectly induce an electrostatic field inside the metal, which may thereby affect the electrostatic potential and the distribution of charges in the metal.

Comparing with the EEC, the MEEC may exhibit some advantages. First, the MEEC may not be restricted to a perfect conductor, and could be valid for any real metal or alloy with noticeable electrical conductivity regardless of the state. So, the MEEC may have a larger application scope than EEC. Second, the physics revealed by the MEEC may be more correct and more appropriate. Third, the MEEC could point out the popular existence of the intrinsic electrostatic field inside a metal and the TEF at the meal surface, which may assist in interpreting the related phenomena in various fields.

2.1.2 Electrostatic boundary conditions (EBCs) for a metal

To solve the electrostatic problems of metals, one usually makes use of the traditional EBC which is given by [1,4,18,19]

$$\begin{cases} \vec{n} \times \vec{E} = 0 \\ \vec{n} \cdot \vec{E} = \sigma/\varepsilon_0\varepsilon, \end{cases} \tag{9}$$

where n denotes the unit vector perpendicular to the metal surface, pointing outwards, E is the electrostatic field at metal surface, σ is the surface charge density, and ε_0 and ε are the vacuum permittivity and relative dielectric constant of the media around the metal, respectively. Nevertheless, both the intrinsic TEF at the metal surface and the intrinsic electrostatic field inside metals [9] may indicate that the EBC may not be applicable for any real metal. So, the rigorous electrostatic boundary conditions (REBC) for a metal should be tackled and they are given by

$$\begin{cases} \vec{n} \times \vec{E} = \vec{n} \times \vec{E}_i(\vec{r})|_{S-0} \\ \vec{n} \cdot \varepsilon_0\varepsilon\vec{E} = \sigma + \vec{n} \cdot \varepsilon_0\varepsilon_m\vec{E}_i(\vec{r})|_{S-0}, \end{cases} \tag{10}$$

where ε_m is the electrostatic dielectric constant for the metal, E is the total electrostatic field outside the metal surface, and $E_i(r)|_{S-0}$ is the intrinsic electrostatic field under the metal surface. As is shown, the TEF at the metal surface is continuous. The electric field outward normal to the metal surface cannot precisely determine the surface charge density and it is also dependent on the intrinsic electrostatic field inward normal to the metal surface. It may be easily found that only when the intrinsic electrostatic field $E_i(r)$ is so weak that it can be ignored, can the REBC be simplified to be the EBC.

For the REBC, the surface charge density may be written as $\sigma = \sigma_e + \sigma_i$, where σ_e is the externally charged

or discharged charge density at the metal surface, and σ_i denotes the intrinsic surface charge density which only depends on the intrinsic electrostatic field distribution, and it may be expressed as follows:

$$\sigma_i = \vec{n} \cdot \varepsilon_0 \varepsilon \vec{E}_i(\vec{r})|_{S+0} - \vec{n} \cdot \varepsilon_0 \varepsilon_m \vec{E}_i(\vec{r})|_{S-0}, \tag{11}$$

where $E_i(r)|_{S+0}$ is the intrinsic electrostatic field above the metal surface. Substituting Eqs. (6), (8), and (11) in Eq. (10), the REBC may be expressed in another form

$$\begin{cases} \vec{n} \times \vec{E}_e(\vec{r}) = 0 \\ \vec{n} \cdot \varepsilon_0 \varepsilon \vec{E}_e(\vec{r}) = \sigma_e. \end{cases} \tag{12}$$

The form of REBC gives the EBC for the electrostatic field $E_e(r)$. A comparison between EBC (Eq. (9)) and REBC (Eq. (12)) may be interesting and enlightening. At first glance, their forms are the same as each other, but their physical meanings may be quite different from each other. EBC demonstrates that the electrostatic field at the metal surface must be normal to the surface, and its magnitude determines the surface charge density. On the contrary, REBC indicates that the externally applied electrostatic field $E_e(r)$ is perpendicular to the metal surface and the electrostatic field $E_e(r)$ at the metal surface is related to the externally charged or discharged surface charge density σ_e.

The REBC not only can lead to complexities and difficulties for solving the electrostatic problems of metals, but can also lead to new understandings of electrostatics of metals.

2.1.3 First uniqueness theorem for metals

The first uniqueness theorem states that "The solution to Laplace's equation in some volume V is uniquely determined if the potential is specified on the boundary surface S" [4,18–20]. Its mathematical form could be expressed as follows [4,18–21]:

$$\begin{cases} \nabla^2 \varphi(\vec{r}) = \rho_e / \varepsilon_0 \varepsilon \\ \varphi(\vec{r})|_S \quad \text{is specified,} \end{cases} \tag{13}$$

where ρ_e is the charge density in the volume V outside the metal. Its mathematical proof is provided in many famous textbooks [4,18–21]. The first uniqueness theorem with Dirichlet boundary condition is valid in mathematics. According to the theorem, if the surface potential $\varphi(r)|s$ can be specified accurately, the solution $\varphi(r)$ in the volume V can also be specified. However, for the application of first uniqueness theorem in electrostatic problems of the real metals, what is commonly known is the external electrostatic potential $\varphi_e(r)$ which cannot solely give the electrostatic potential of the metal. The electrostatic potential may be dominated by both the external electrostatic potential $\varphi_e(r)$ and the intrinsic electrostatic potential $\varphi_i(r)$, as is indicated by Eq. (5). So, the corresponding surface potential of the metal should be given by

$$\varphi(r)|_S = \varphi_i(r)|_S + \varphi_e(r)|_S, \tag{14}$$

where $\varphi(r)|_S$ stands for the precise electrostatic potential at the metal surface, and $\varphi_i(r)|_S$ and $\varphi_e(r)|_S$ denote the intrinsic electrostatic potential and external electrostatic potential at the metal surface, respectively. As indicated previously, $\varphi_e(r)|_S$ does not exhibit position dependence and is a constant at the metal surface, but $\varphi_i(r)|_S$ is usually position dependent. The intrinsic electrostatic potential $\varphi_i(r)$ may be very hard to obtain, because the correlated Fermi level usually depends on many complex unspecified factors, *e.g.*, the residual stresses, surface reconstruction, composition distribution, and the number and distribution of various defects. For the intrinsic electrostatic potential, it can be concluded that it may rest with the distribution of intrinsic electrostatic charges in the metal and it may satisfy the relation $\nabla^2 \varphi_i(\vec{r}) = 0$ in the concerned volume V outside the metal. In another respect, when applying the first uniqueness theorem for a metal, one generally only considers the external electrostatic potential $\varphi_e(r)|_s$ but neglects the intrinsic electrostatic potential $\varphi_i(r)|_s$ at the metal surface. As a result, the uniqueness theorem in the actual electrostatic problems of a metal becomes

$$\begin{cases} \nabla^2 \varphi_e(\vec{r}) = \rho_e / \varepsilon_0 \varepsilon \\ \varphi_e(\vec{r})|_S = \text{constant.} \end{cases} \tag{15}$$

The solution is unique and the proof is simple and shown as follows. The functions $\varphi_{e1}(r)$ and $\varphi_{e2}(r)$ are supposed to be the solutions. Let the function U be $U = \varphi_{e1}(r) - \varphi_{e2}(r)$. The function U satisfies the following dominant equation and Dirichlet boundary condition according to Eq. (15):

$$\begin{cases} \nabla^2 U = 0 \\ U|_S = 0 \end{cases}$$

Using the identity equation for arbitrary scalar field ψ,

$$\int_V \psi \nabla^2 \psi + \nabla \psi \cdot \nabla \psi \mathrm{d}v = \oint_S \psi \frac{\partial \psi}{\partial n} \mathrm{d}s. \tag{16}$$

The function U satisfies the following equation:

$$\int_V (\nabla U)^2 + U \nabla^2 U \mathrm{d}v = \oint_S U \frac{\partial U}{\partial n} \mathrm{d}s.$$

Using the dominant equation and Dirichlet boundary condition for U, the above equation changes to

$$\int_V (\nabla U)^2 \mathrm{d}v = 0,$$

which implies $\nabla U = 0$. Consequently, the function U is a constant inside the concerned volume V. For Dirichlet boundary condition of the function U, *i.e.*, $U = 0$ at the metal surface, U must be zero inside the volume V so that $\varphi_{e1}(r) = \varphi_{e2}(r)$ and the solution of Eq. (15) is unique. As is shown, the precise solution is the external electrostatic potential including the contribution of induction charges at the metal surface. But it does not contain the contribution of the intrinsic electrostatic potential $\varphi_i(r)$ in the volume V, so it is only a rough approximation for the electrostatic problem. Under the approximation, the far-field solution may be relatively accurate because the intrinsic electrostatic potential $\varphi_i(r)$ usually decays rapidly and almost vanishes in the far-field regions. However, the near-field solution may show a very noticeable deviation because the intrinsic electrostatic potential $\varphi_i(r)$ may display a notable magnitude in the near-field regions. Therefore, the intrinsic electrostatic potential $\varphi_i(r)$ and the related intrinsic electrostatic field $E_i(r)$ must be taken into account when one will carry out the investigations on near-field physics and chemistry, especially the surface physics and surface chemistry. Here the words "far-field" and "near-field" refer to the concerned regions far away from the metals and the concerned regions in the vicinity of the metals, respectively.

2.1.4 Second uniqueness theorem for metals

The second uniqueness theorem states that "In a volume V surrounded by metals and containing a specified charge density ρ_e, the electric field is uniquely determined if the total charge on each conductor is given" [4,19,21]. Its mathematical form could be given by [4,19]

$$\begin{cases} \nabla^2\varphi(\vec{r}) = \rho_e/\varepsilon_0\varepsilon \\ -\varepsilon_0\varepsilon\int_S \dfrac{\partial\varphi(\vec{r})}{\partial n}\mathrm{d}s = Q, \end{cases} \tag{17}$$

where Q denotes the total charge on a metal. The mathematical proof is available in many classical textbooks on electrodynamics [4,19,21]. As shown in Eq. (5), the solution for the total electrostatic potential $\varphi(r)$ is composed of the external electrostatic potential $\varphi_e(r)$ and the intrinsic electrostatic potential $\varphi_i(r)$. Indicated by the MEEC, the metal may not be an equipotential body for the total potential $\varphi(r)$, so the common mathematical proof [4,19,21] based on the EEC that the metal is an equipotential body may not hold right. The proof may be simple. The function $\varphi_1(r)$ is supposed to be a solution of Eq. (17). The function $\varphi_1(r) + a\varphi_i(r)$ (a is an arbitrary nonzero constant) must be another solution if the function $\varphi_i(r)$ satisfies

$$\begin{cases} \nabla^2\varphi_i(\vec{r}) = 0 \\ -\varepsilon_0\varepsilon\int_S \dfrac{\partial\varphi_i(\vec{r})}{\partial n}\mathrm{d}s = 0. \end{cases} \tag{18}$$

One may also easily find that there are many nontrivial solutions for the problem described by Eq. (18), which is shown in Figure 3. In other words, the mathematical solution of the problem stated by the traditional second uniqueness theorem on metals is not unique and thus the second uniqueness theorem is not established rigorously in the viewpoint of mathematics.

Despite the faults of the traditional second uniqueness theorem in mathematics, it could still be useful in physics. When the position-dependent intrinsic electrostatic potential $\varphi_i(r)$ is unique and precisely known, the corresponding solutions $\varphi_e(r)$ and $\varphi(r)$ could be determined uniquely. In many real situations, a metal is intrinsically neutral and thereby the totally intrinsic electrostatic charge in the metal is zero, which means that the intrinsic electrostatic potential $\varphi_i(r)$ satisfies Eq. (18). Simultaneously, as analyzed in Section 2.1.3, the intrinsic electrostatic charges may reside in the metal and thus the potential $\varphi_i(r)$ may conform to the relation $\nabla^2\varphi_i(\vec{r}) = 0$ in the volume V outside the metal. As a result, the mathematical form of the *second uniqueness theorem* on metals changes into the following form by means of Eqs. (5), (14), and (18):

$$\begin{cases} \nabla^2\varphi_e(\vec{r}) = \rho_e/\varepsilon_0\varepsilon \\ -\varepsilon_0\varepsilon\int_S \dfrac{\partial\varphi_e(\vec{r})}{\partial n}\mathrm{d}s = Q. \end{cases} \tag{19}$$

In view of the MEEC that the external electrostatic potential $\varphi_e(r)$ is equipotential in the whole metal body,

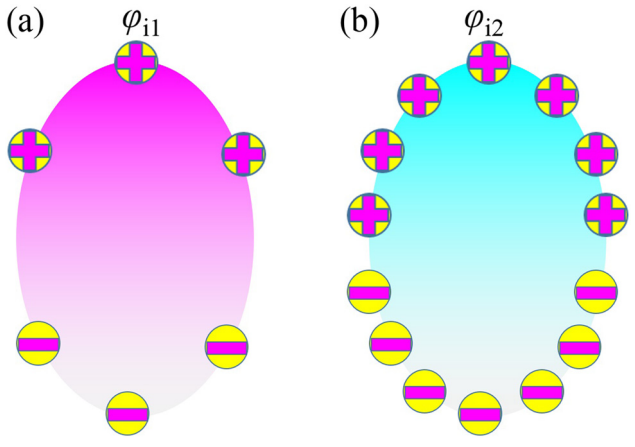

Figure 3: The distribution of intrinsic charges at the totally neutral metal surfaces. (a) Little intrinsic charges at the metal surfaces with the corresponding electrostatic potential $\varphi_{i1}(r)$; and (b) more intrinsic charges at the metal surfaces with the electrostatic potential $\varphi_{i2}(r)$.

it could be found that the solution is unique based on the same mathematical proof method in the textbooks [4,19,21]. The related proof is offered here. The external electrostatic potential functions $\varphi_{e1}(r)$ and $\varphi_{e2}(r)$ are supposed to be the solutions. Let the function U be $U = \varphi_{e1}(r) - \varphi_{e2}(r)$ and the function U satisfies the dominant equations

$$\begin{cases} \nabla^2 U = 0 \\ \int_S \frac{\partial U}{\partial n} \mathrm{d}s = 0. \end{cases}$$

Using the identity equation shown by Eq. (16) the function U fulfills the following equation:

$$\int_V (\nabla U)^2 \mathrm{d}v = \oint_S U \frac{\partial U}{\partial n} \mathrm{d}s.$$

As pointed out by the MEEC, the external electrostatic potentials $\varphi_{e1}(r)$ and $\varphi_{e2}(r)$ are constant potentials at the metal surface, so the function U is also a constant at the metal surface S. As a result, the above equation can be written as follows:

$$\int_V (\nabla U)^2 \mathrm{d}v = U \oint_S \frac{\partial U}{\partial n} \mathrm{d}s.$$

Using the boundary condition of the function U, the above equation becomes

$$\int_V (\nabla U)^2 \mathrm{d}v = 0,$$

which implies $\nabla U = 0$ and U is a constant in the concerned volume V, meaning that the solution is unique apart from an unimportant arbitrary additive constant.

Therefore, the second uniqueness theorem for metals exactly describes the external electrostatic potential $\varphi_e(r)$ instead of the total electrostatic potential $\varphi(r)$. To be noted is that the discussed external electrostatic potential $\varphi_e(r)$ contains the contributions of both the induction charges in the metal and the stationary charges in the concerned volume V outside the metal.

For the applications of the second uniqueness theorem in the actual electrostatic problems of metals, like the case of the first uniqueness theorem, people usually neglect the important role of the intrinsic electrostatic potential $\varphi_i(r)$. Hence, the obtained solution may be the external electrostatic potential $\varphi_e(r)$. It may be a relatively good solution in the far-field regions but need a careful correction in the near-field regions, as is in analogy with the case of first uniqueness theorem.

If the electrostatic problem is given by Robin's boundary condition shown below

$$\begin{cases} \nabla^2 \varphi(\vec{r}) = \rho_e / \varepsilon_0 \varepsilon \\ \left[\alpha \varphi(\vec{r}) + \beta \frac{\partial \varphi(\vec{r})}{\partial n} \right] \Big|_S \text{ are specified,} \end{cases}$$

where α, β are two arbitrary real constants with the same sign. The solution is also unique in mathematics. The proof is simple and presented as follows. Let the functions φ_1 and φ_2 be two solutions. Let the function U be $U = \varphi_1 - \varphi_2$. The function U satisfies

$$\begin{cases} \nabla^2 U = 0 \\ \left[\alpha U + \beta \frac{\partial U}{\partial n} \right] \Big|_S = 0. \end{cases}$$

Using the identity Eq. (16) the function U fulfills

$$\int_V (\nabla U)^2 \mathrm{d}v = \oint_S U \frac{\partial U}{\partial n} \mathrm{d}s.$$

Inserting Robin's boundary condition will yield

$$\int_V (\nabla U)^2 \mathrm{d}v = \oint_S -\frac{\alpha}{\beta} U^2 \mathrm{d}s.$$

Since α, β are two arbitrary constants with the same sign, the above equation holds right only when the difference function U is zero. Therefore, the solution is unique. When the electrostatic problems of metals with Robin's condition is solved, the contribution of the intrinsic electrostatic potential $\varphi_i(r)$ should be included.

In another respect, sometimes what is encountered is the electrostatic problem that exhibits the mixed boundary condition, *i.e.*, Dirichlet boundary condition over a part of the metal surface $S1$ and Neumann boundary condition over the remaining part $S2$, as is represented by the following equation:

$$\begin{cases} \nabla^2 \varphi(\vec{r}) = \rho_e / \varepsilon_0 \varepsilon \\ \varphi(\vec{r})|_{S1} \text{ and } -\varepsilon_0 \varepsilon \frac{\partial \varphi(\vec{r})}{\partial n} \Big|_{S2} \text{ are specified.} \end{cases}$$

Its mathematical solution is also unique. The proof is almost the same as the proof for uniqueness theorem. To be noted is that the solution $\varphi(r)$ is not an equipotential at the part of metal surface $S1$ and it should contain the contribution of intrinsic electrostatic potential $\varphi_i(r)$. On the other hand, what the boundary condition gives is not the surface charge density at the remaining part of metal surface $S2$. If the electrostatic problem of metals is described by the mixed boundary conditions in the following mathematical form:

$$\begin{cases} \nabla^2 \varphi(\vec{r}) = \rho_e / \varepsilon_0 \varepsilon \\ \varphi(\vec{r})|_{S1} \text{ and } -\varepsilon_0 \varepsilon \int_{S2} \frac{\partial \varphi(\vec{r})}{\partial n} \mathrm{d}s \text{ are specifed,} \end{cases}$$

the solution is not unique in mathematics because the accurate potential $\varphi(r) = \varphi_e(r) + \varphi_i(r)$ at the metal surface $S2$ is not a constant. And there are many solutions for the problem. The proof is similar to that of the traditional second uniqueness theorem for metals. On the contrary, if the problem is given by the mixed boundary condition shown below, then

$$\begin{cases} \nabla^2\varphi_e(\vec{r}) = \rho_e/\varepsilon_0\varepsilon \\ \varphi_e(\vec{r})|_{S1} \text{ and } -\varepsilon_0\varepsilon\int_{S2}\frac{\partial\varphi_e(\vec{r})}{\partial n}ds \text{ are specifed,} \end{cases}$$

the solution is unique because the external electrostatic potential $\varphi_e(r)$ is a constant potential over the metal surfaces $S1$ and $S2$. In other words, what the traditional *Unique theorem* with the above mixed boundary condition uniquely gives is the external electrostatic potential $\varphi_e(r)$ not the accurate potential $\varphi(r)$.

The above discussions on uniqueness theorem (first uniqueness theorem and second uniqueness theorem) may not only point out the faults but also generate some new knowledge in related areas. On one hand, it may inspire people to realize the crucial role of the intrinsic electrostatic potential and the intrinsic electrostatic field in some scientific areas, particularly the surface physics and surface chemistry. On the other hand, the new understandings of the uniqueness theorem will subsequently give birth to new knowledge of the classical method of image charges and the famous electrostatic shielding in electrodynamics, which is addressed in the later part of the article.

2.1.5 Method of image charges

The method of image charges is popularly utilized to solve many electrostatic problems of metals. Its validity builds upon the uniqueness theorem. Its introduction and applications in electrostatic problems of metals could be found in some textbooks on electrodynamics [1,4,18,19,22,23]. As is demonstrated, if the solution not only satisfies Poisson's equation in the concerned volume but also gives the correct EBC, it must be right. However, for the applications of the method in the related electrostatic problem, the commonly obtained solution may either satisfy Eq. (15) or Eq. (19), completely neglecting the contribution of the intrinsic electrostatic potential of the metal in the concerned volume. Therefore, as discussed for uniqueness theorem in the preceding sections, the solution that is obtained based on the method of image charges is the external electrostatic potential $\varphi_e(r)$ rather than the precise electrostatic potential $\varphi(r)$ shown in Eq. (5). Hence, the method of image charges may be an approximation. The approximation may be satisfactory in the far-field regions but it may need to be corrected in the near-field regions, which should be paid attention to for the surface-science researchers.

2.1.6 Electrostatic shielding

Electrostatic shielding can create a volume for protecting any concerned electric devices and instruments from the effect of any external electrostatic field. It is well-known and has been widely applied in various fields for more than 200 years up to now. For example, it was employed to accomplish the precise test of Coulomb's law by many scientists in different generations, *e.g.*, Cavendish (1773) [24], Maxwell (1873) [24], Plimpton and Lawton [25], and Williams *et al.* [26]. Wherein Williams *et al.* [26] achieved a miraculously precise upper limit on the deviation $\delta = (2.7 \pm 3.1) \times 10^{-16}$ which was commonly used to certify Coulomb's inverse square law in the form $1/r^{2+\delta}$.

In electrodynamics, the electrostatic shielding states that the electrostatic field is precisely zero in the empty cavity of a closed metal surface [1,21,27]. The conclusion builds on the first uniqueness theorem and the traditional EEC that the electrostatic field inside a metal must be null [27]. On the contrary, as concluded by the previous sections, the MEEC and uniqueness theorem for metals suggest that what must be null and unique is the electrostatic field induced by the external electrostatic potential, but the macroscopic intrinsic electrostatic field stemming from position-dependent Fermi level may be allowed to sustain inside the metal. As a consequence, the non-null intrinsic electrostatic field $E_i(r)$ and related intrinsic electrostatic potential $\varphi_i(r)$ may exert on the empty cavity of a closed metal surface, which is schematically shown in Figure 1. In other words, a real metal popularly presents net charges in some regions and displays a net electrostatic field in the empty cavity enclosed by the metal, but both of them are very difficult to eliminate. So, the electrostatic shielding can shield any external electrostatic field but cannot shield the intrinsic electrostatic field of the metal no matter how strong or weak the intrinsic electrostatic field is.

The question is why the intrinsic electrostatic field $E_i(r)$ and intrinsic electrostatic potential $\varphi_i(r)$ does not usually influence the related electrostatic shielding experiments. It may be attributed to the following reasons. First, the position-dependent Fermi level in a metal may not be altered under the commonly external electrostatic field and the related potential. So, the corresponding intrinsic electrostatic field $E_i(r)$ would not vary in the metal and cannot give rise to the electromagnetic effect. Second, the concerned electric devices and instruments in the cavity may usually be put in the far-field regions where the

intrinsic electrostatic field $E_i(r)$ may be too weak to be detected. To the contrary, if the concerned devices would vibrate in the near-field regions of the cavity, an electrical induction current might emerge and a weak electromagnetic wave might be radiated simultaneously.

2.1.7 Thomson's theorem

Thomson's theorem states that "Static charge on a system of perfect conductors distribute itself so that the electric stored energy is minimum" [20], where the "perfect conductor" refers to "a material that has many free charges to move under external influences, electric or non-electric" [20]. The mathematical proof of Thomson's theorem could be found in some textbooks on electrodynamics [18,20]. Thomson's theorem and the corresponding proof only considers the external electrostatic potential $\varphi_e(r)$ but omits the vital role of the intrinsic electrostatic potential $\varphi_i(r)$ and the intrinsic electrostatic field $E_i(r)$. Considering both the electrostatic potentials, the total electrostatic energy stored in the system should be given by

$$W_t = \frac{\varepsilon_0\varepsilon_m}{2}\int_{V_m}[\nabla\varphi_i(\vec{r}) + \nabla\varphi_e(\vec{r})]^2 dV + \frac{\varepsilon_0\varepsilon}{2}\int_{V}[\nabla\varphi_i(\vec{r}) + \nabla\varphi_e(\vec{r})]^2 dV, \quad (20)$$

where W_t denotes the totally stored electrostatic energy in the metal systems, V_m is the volume of the metal systems, and V is the concerned volume outside the metal systems. It could be written as the summation of the following three types of electrostatic energies:

$$W_t = W_i + W_e + W_{ie},$$

$$W_i = \frac{\varepsilon_0\varepsilon_m}{2}\int_{V_m}[\nabla\varphi_i(\vec{r})]^2 dV + \frac{\varepsilon_0\varepsilon}{2}\int_{V}[\nabla\varphi_i(\vec{r})]^2 dV,$$

$$W_e = \frac{\varepsilon_0\varepsilon_m}{2}\int_{V_m}[\nabla\varphi_e(\vec{r})]^2 dV + \frac{\varepsilon_0\varepsilon}{2}\int_{V}[\nabla\varphi_e(\vec{r})]^2 dV,$$

$$W_{ie} = \varepsilon_0\varepsilon_m\int_{V_m}\nabla\varphi_i(\vec{r})\cdot\nabla\varphi_e(\vec{r})dV + \varepsilon_0\varepsilon\int_{V}\nabla\varphi_i(\vec{r})\cdot\nabla\varphi_e(\vec{r})dV,$$

where W_i stands for the intrinsic electrostatic energy contributed by the intrinsic electrostatic potential $\varphi_i(r)$ and the intrinsic electrostatic field $E_i(r)$, W_e is the electrostatic energy arising from the external electrostatic potential $\varphi_e(r)$ and the external electrostatic field $E_e(r)$, W_{ie} is the interaction energy between the two fields.

According to the MEEC in Section 2.1.1, the potential $\varphi_e(r)$ is constant and the field $E_e(r)$ is null inside the metal, *i.e.*, $\nabla\varphi_e(r) = 0$. So, the interaction energy W_{ie} could be expressed as follows:

$$W_{ie} = \varepsilon_0\varepsilon\int_{V}\nabla\varphi_i(\vec{r})\cdot\nabla\varphi_e(\vec{r})dV.$$

The intrinsic electrostatic charges are distributed within the metal such that the potential fulfills the relation $\nabla^2\varphi_i(r) = 0$ in the volume V outside the metal systems. Using the equation $\nabla\varphi_e(r)\cdot\nabla\varphi_i(r) = \nabla[\varphi_e(r)\nabla\varphi_i(r)] - \varphi_e(r)\nabla^2\varphi_i(r)$, the interaction energy W_{ie} may be written as follows:

$$W_{ie} = \varepsilon_0\varepsilon\int_{S}\varphi_e(\vec{r})\nabla\varphi_i(\vec{r})dS,$$

$$W_{ie} = \sum Q_i\varphi_e(\vec{r})|_s, \quad (21)$$

where Q_i is the totally intrinsic charges in the metal, and S is the closed surface of the volume V outside the metal systems. The non-charged metal may inherently be neutral and the totally intrinsic charges inside the metal may be zero, *i.e.*, $Q_i = 0$. Thus, the interaction energy W_{ie} may be zero. In general, during the charging or discharging processes of a metal, the yielded electric force exerted on the metal may be so weak that the microstructure and Fermi level may not vary. Therefore, the intrinsic electrostatic energy W_i may be an invariable quantity for the definite metal systems. As a consequence, the distribution of charged charges at the metal surface influences the incremental electrostatic energy W_e.

$$W_e = \frac{\varepsilon_0\varepsilon}{2}\int_{V}[\nabla\varphi_e(\vec{r})]^2 dV. \quad (22)$$

It may be easily found that if the metal is an equipotential body for the external electrostatic potential $\varphi_e(r)$, the stored electric energy W_e is minimum. The corresponding proof may be the same as that in many textbooks on electrodynamics [18,20].

According to the above discussions, the famous Thomson's theorem may be modified as "Charged net charges on a system of real metals distribute themselves so that the incremental electric energy is minimum." This modification may bring several merits. First, unlike Thomson's theorem applicable for perfect conductors, the modified Thomson's theorem may be valid for both perfect conductors and real metals. In other words, the application scope of the modified Thomson's theorem is much larger than that of Thomson's theorem. Second, considering the existence of intrinsic electrostatic field and the stored electric energy, the statement of the modified Thomson's theorem may be more accurate than that of Thomson's theorem.

2.1.8 Green's reciprocation theorem

Green's reciprocation theorem is usually expressed in the following form [18,20]:

$$\sum_{k=1}^{n} q_k' \varphi_k = \sum_{k=1}^{n} q_k \varphi_k',$$

where φ_k is the electrostatic potential of the kth metal when it carries charge q_k, and φ_k' is the potential when it carries charge q_k'. The proof could be available in the textbooks on electrodynamics [18,20]. Green's reciprocation theorem is very useful in solving many electrostatic problems of metals. However, as revealed by MEEC, the position-dependent intrinsic electrostatic potential $\varphi_i(r)$ was usually omitted for a metal and the metal may not be an equipotential body for the total electrostatic potential. To one's surprise, it means that any constant potential cannot accurately describe the total electrostatic potential of a metal. So, the popular form of Green's reciprocation theorem may not be appropriate and has to be modified for wide applications. In actual applications, the known potential of a metal is usually the external electrostatic potential $\varphi_e(r)$. It is a constant potential for the metal and satisfies the relation $\nabla^2\varphi_e(r) = 0$ outside the metals, so the Green's reciprocation theorem may better be modified as

$$\sum_{k=1}^{n} Q_k' \varphi_{ek} = \sum_{k=1}^{n} Q_k \varphi_{ek}', \tag{23}$$

where φ_{ek} is the external electrostatic potential of the kth metal when it carries charge Q_k, and φ_{ek}' is the external electrostatic potential when it carries charge Q_k'. The mathematical proof may be the same as that in the related textbooks [18,20].

The modified Green's reciprocation theorem could be utilized to solve the related electrostatic problems of metals. By modifying Green's reciprocation theorem, we can obtain the external electrostatic potential rather than the total electrostatic potential of the metal body. If the investigated topics are associated with physics and chemistry at metal surfaces, the intrinsic electrostatic potential of the metal must be taken into account seriously.

2.2 Physical effects of TEF

2.2.1 Electric transport properties at surfaces

As shown in Figure 4, when an external voltage is applied to the metal surface with different Fermi levels, an electrical circuit may be formed. In analogy with the situation for the metal with different Fermi levels [5], the electrical current–voltage (I–V) relation of the metal surface may exhibit rectifying characters. If a forward bias external voltage is applied as shown in Figure 4(a), the energy of free electrons in region III may be uplifted relative to that of free electrons in region I, so that free electrons would drift from region III to region I, creating an electrical current which is displayed in Figure 4(c). However, upon application of a small backward bias voltage shown in Figure 4(b), the electrical current may be almost zero except a tiny tunneling current, because the free electron movement may be blocked by the energy barrier originating from the Fermi level difference. If the backward bias voltage increases to a critical value V_Z, the free electrons in region I may gain enough energy to surpass the energy barrier and reach region III easily, thereby forming a notable electrical current, as shown in Figure 4(c). And the critical voltage V_Z could be obtained according to Eq. (1) as follows:

$$V_Z = -\frac{1}{e}[E_F(\vec{r}_{III}) - E_F(\vec{r}_I)], \tag{24}$$

where e is the electron charge, and $E_F(\vec{r}_{III})$ and $E_F(\vec{r}_I)$ are the Fermi levels of region III and region I, respectively. It means that in the presence of TEF, the metal surfaces sometimes could rectify electrical current and behave as a p–n junction. And the rectifying characters may be more obvious at low temperatures because of the suppression of thermal excitation.

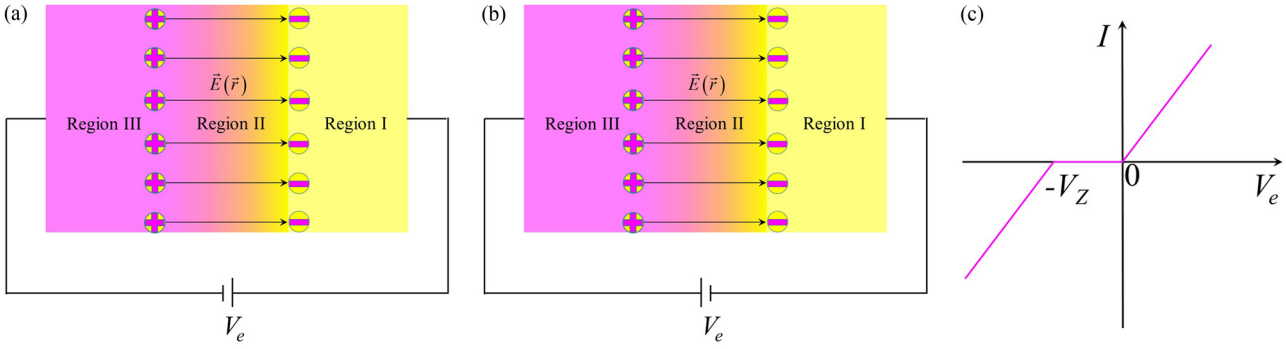

Figure 4: Electrical current–voltage (I–V) relation for the metal surface with a TEF. Region I (colored yellow) and region III (colored magenta) denote places with lower Fermi level and higher Fermi level, respectively, while region II shows the transition zone between region I and region III. (a) forward bias voltage; (b) backward bias voltage; and (c) I–V characteristics.

For actual metal surfaces, the complex strains, adsorptions, defects, and so on may induce very complex TEF. As revealed, the fields could cause the rectifying characters and usually reduce the surface electrical conductivity. It may enlighten people that to obtain a relatively precise electrical conductivity of metal surface, one had better employ a large electrical voltage to measure in both ways of forward bias and backward bias and take the larger value of conductivity.

2.2.2 Rashba effect at the metal surface

The Rashba effect first discovered in 1959 describes a momentum-dependent spin splitting of electron states in a bulk crystal [28] and low dimensional electron systems [29]. For an electron system with space inversion-symmetry breaking, it is commonly described by the following Hamiltonian:

$$|H_R = \alpha_R \vec{n} \cdot(\hat{\sigma} \times \vec{k}), \tag{25}$$

where $\vec{k}$ is the electron momentum, $\hat{\sigma}$ is the Pauli matrices, $\vec{n}$ is the unit vector normal to the surface, and the parameter α_R is Rashba coupling which is usually proportional to the magnitude of electric field.

Based on the physics of Rashba effect, the TEF at metal surface may also contribute to the momentum-dependent spin splitting of electron bands, and the correlated Hamiltonian may be given by

$$H_{RZ} = \eta \nabla E_F \cdot(\hat{\sigma} \times \vec{k}), \tag{26}$$

where η is the coupling parameter with the unit m^2. Appearance of this Hamiltonian may further reduce the symmetry of electron spin bands in the momentum space. To examine its effect, the total Hamiltonian of the electrons should contain the kinetic energy of the electron, the conventional Hamiltonian for Rashba effect, and the Hamiltonian term H_{RZ} originating from the TEF at the metal surface. So, the total Hamiltonian could be written as follows:

$$H_R = \frac{p^2}{2m_e} + \alpha_R \vec{n} \cdot(\hat{\sigma} \times \vec{k}) + \eta \nabla E_F \cdot(\hat{\sigma} \times \vec{k}), \tag{27}$$

where the first term on the right hand is the kinetic energy of the electron and p signifies the momentum operator. In terms of simple calculation, the eigenenergy is as follows:

$$|E_{\pm}(\vec{k}) = \frac{\hbar^2 k^2}{2m_e} \pm |(\alpha_R \vec{n} + \eta \nabla E_F) \times \vec{k}|. \tag{28}$$

It shows that the momentum-dependent splitting of electron band may be shifted in the presence of TEF. When the tangential field would vanish, the related eigenenergy would reduce to the familiar solutions for the Rashba Hamiltonian, as inversely verifies the correctness of the above electron bands given by Eq. (28).

Due to the TEF in Eq. (26), a spin component normal to the surface will appear as

$$\langle \varphi_1 | S_Z | \varphi_1 \rangle = \frac{\hbar}{2} \frac{\eta(\vec{k} \times \nabla E_F) \cdot \vec{n}}{|(\alpha_R \vec{n} + \eta \nabla E_F) \times \vec{k}|}, \tag{29}$$

where $|\varphi_1\rangle, \langle \varphi_1|$ is the eigenket and eigenbra, respectively, and S_Z is the spin component normal to the surface.

Generally speaking, the magnitude of tangential field in many metals may not be so strong that its effect might be weaker than Rashba effect. But for some special situations where the Rashba Hamiltonian vanishes, *i.e.*, the zero Rashba coupling α_R, the eigenenergy for the 2D electron systems would be

$$E_{\pm}(\vec{k}) = \frac{\hbar^2 k^2}{2m_e} \pm |\eta \nabla E_F \times \vec{k}|. \tag{30}$$

The effective magnetic field is

$$\vec{B}_{eff} = \frac{2\eta}{g\mu_B}(\nabla E_F \times \vec{k}), \tag{31}$$

where g is the spin-g factor and has a value of about 2, and μ_B is the Bohr magneton. And the related electron spin component along surface normal is

$$\langle \varphi_1' | S_Z | \varphi_1' \rangle = \frac{\hbar}{2} \frac{\eta(\vec{k} \times \nabla E_F) \cdot \vec{n}}{|\eta \nabla E_F \times \vec{k}|}, \tag{32}$$

where $|\varphi_1'\rangle$, $\langle \varphi_1'|$ is the corresponding eigenket and eigenbra, respectively. Very interestingly, for a 2D electron system even without magnetic field, if the electrons only possess the momentum parallel to the surface and the normal component is zero, the presence of any TEF would give birth to a totally spin-polarized state and the electron spin polarization strongly depends on its momentum. At ground state, the electron spins are polarized and parallel to the effective magnetic field B_{eff} as shown in Figure 5. The effective magnetic field and related spin splitting energy might be detected by means of electron spin resonance experiments which were successfully carried out to measure the spin splitting energy for a 2D electron system [30]. For such a 2D electron system as displayed in Figure 5(a), the up spins would accumulate on the left side, while the down spins would get together on the right side of the metal surface. On application of an external electrical voltage at metal surface, only the electrons with up spin are allowed to flow but the electrons with down spin are inhibited as illustrated by Figure 5(b). Hence, the metal surface with the TEF might be a platform for anomalous quantum Hall effect.

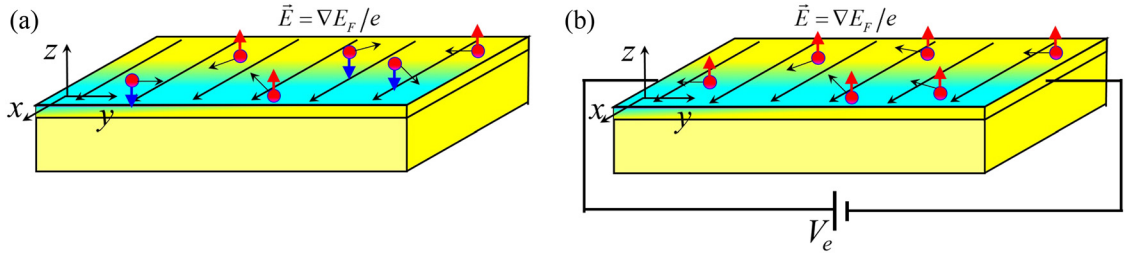

Figure 5: Momentum dependence (short black arrows) of polarized electron spins under a TEF at the metal surface. The tangential field is along the *x* axis as indicated by the long black arrows. The red circles present the electrons. Red arrows and blue arrows denote the polarization direction of electron spins. (a) without external electrical voltage; and (b) with an electrical voltage V_e.

2.2.3 Effect on the photoemission spectroscopy (PES)

According to electrostatics [1,4], *i.e.*, circumstances in which no physical variables depend on time, one may have

$$\nabla \times \vec{E} = 0. \tag{33}$$

So the TEF along the metal surface may cause a related tangential component outside the surface as illustrated by black arrows in Figure 2. It may have an important effect on PES.

Based on the physical theory of PES [31], a tangential field may affect PES in two ways. One is that it may change the detected kinetic energy of photoelectrons by the quantity.

$$\Delta E_{\text{kin}} = eV_0, \tag{34}$$

where ΔE_{kin} is the variation in kinetic energy of photoelectron, e is the electron charge, and V_0 is the potential difference between the positions of photoelectron emission point and electron analyzer. As shown in Figure 6, because of the complexity for both the experimental design and the unknown distribution of TEF in real experimental metal surface, the precise value of kinetic energy variation may be difficult to get. But one may estimate its value as follows:

$$|\Delta E_{\text{kin}}| \le |E_{\text{F}}(\vec{r}_{\text{III}}) - E_{\text{F}}(\vec{r}_{\text{I}})|. \tag{35}$$

The other is that for the photoelectrons emitting out of the surface, the tangential field may result in alterations for their wave-vector component parallel to the surface. It is

$$k_{||}^{\text{f}} = \sqrt{(k_{||}^{\text{i}})^2 + 2m_e eV_{||}/\hbar^2}, \tag{36}$$

where m_e is the electron mass, $\hbar$ is the reduced Planck's constant, $k_{||}^{\text{i}}$ and $k_{||}^{\text{f}}$, respectively, denote the wave-vector component parallel to the surface for the initial state and final state of a photoelectron, and $V_{||}$ is the potential difference between photoelectron emission point and electron analyzer and it is $V_{||} = -\int_{r_{\text{f}}}^{r_{\text{i}}} \vec{E}_{||}(\vec{r})\cdot d\vec{r}$, where $\vec{E}_{||}(\vec{r})$ is position-dependent TEF outside metal surface, and r_{f}, r_{i} present positions of electron analyzer and photoelectron emission site, respectively. As indicated, the tangential field can indeed change the wave-vector component parallel to the surface. Despite lack of knowledge on the detailed electrostatic field near the metal surface, an estimation could be made and the alteration may be in the range

$$|(k_{||}^{\text{f}})^2 - (k_{||}^{\text{i}})^2| \le \frac{2m_e}{\hbar^2}|E_{\text{F}}(\vec{r}_{\text{III}}) - E_{\text{F}}(\vec{r}_{\text{I}})|. \tag{37}$$

In view of Eqs. (35) and (37), one may find that a larger Fermi level difference and thus a stronger TEF at the metal surface usually have a more notable effect on the PES. Even for the single-crystalline surface at a uniform temperature, there still exists the unavoidable strains arising from residual stresses and defects. For instance, the residual stresses are often reported to reach ~10^2 MPa [13,14,32,33], which can yield a few thousandths of a strain [34]. For most metals, the mechanical-electric coupling strength $|\partial E_{\text{F}}/\partial \xi_{ii}|$ (ξ_{ii} is the main strain) may be in the range 1–10 eV. So the residual strains at the metal surfaces could cause the order of 10 mV for the surface potential variations, which is consistent with

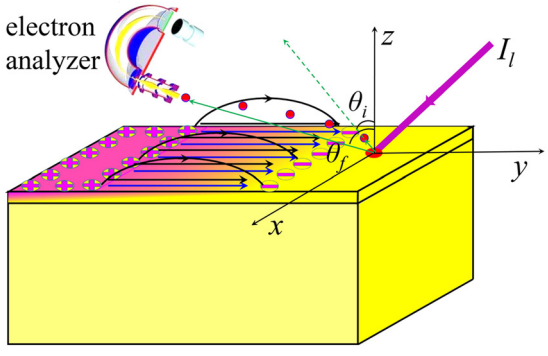

Figure 6: Sketch of PES affected by TEF at the metal surface. When a light beam (colored purple) radiates at the metal surface, some photoelectrons (red dots) would be emitted and their motion would be influenced by the electrostatic field near the surface.

the experimental observations [8,35]. The magnitude of the surface potential variations may place a noticeable restriction on the measurement precision of PES, which deserves attention in the related experiments, *e.g.*, angle-resolved photoemission spectroscopy (ARPES).

The existence of the TEF at the metal surface may hybridize the electron orbital wave functions, for instance, hybridization of s and p orbitals. According to the quantum perturbation theory, the hybridized s and p wave functions are (to first-order precision) as follows:

$$\psi'_{\mathrm{ns}} \approx \psi_{\mathrm{ns}} + \sum \frac{\langle \psi_{\mathrm{np}} | e\vec{E} \cdot \vec{r} | \psi_{\mathrm{ns}} \rangle}{E_{\mathrm{ns}} - E_{\mathrm{np}}} \psi_{\mathrm{np}}, \tag{38}$$

$$\psi'_{\mathrm{np}} \approx \psi_{\mathrm{np}} + \frac{\langle \psi_{\mathrm{ns}} | e\vec{E} \cdot \vec{r} | \psi_{\mathrm{np}} \rangle}{E_{\mathrm{np}} - E_{\mathrm{ns}}} \psi_{\mathrm{ns}}, \tag{39}$$

where Ψ_{ns} and Ψ_{np} are the electron wave functions with main quantum number n and angular momentum s, p, and Ψ'_{ns}, Ψ'_{np} stand for the corresponding hybridized wave functions, respectively.

This hybridization may affect the PES of the metal surface. If the TEF is along x axis, the hybridization only exists between s and p_x electron orbitals. So, the corrected p_x wave function has a component of s orbital wave function. For a tetragonal metal surface with conductive p electrons, a beam of photons can be utilized to radiate the metal surface at a very small glancing angle (*e.g.*, less than 5°) as shown in Figure 7. According to the ARPES theory [36], the measured ARPES intensity may be proportional to the square $|\langle \Psi_{\mathrm{f}} | \vec{A} \cdot \vec{P} | \Psi_{\mathrm{np}} \rangle|^2$, *i.e.*, $I \propto |\langle \Psi_{\mathrm{f}} | \vec{A} \cdot \vec{P} | \Psi_{\mathrm{np}} \rangle|^2$, where A is the electromagnetic gauge and P is the electron momentum. Considering the photon radiation at the metal surface with tetragonal symmetry, the symmetry analysis could be used to clarify the contributions to the APRES intensity. If the glancing photons have s polarization (the photon electric field perpendicular to the scattering plane k_x–k_z), the ARPES intensity contributed by the scattering matrix element is zero along k_y direction $|\langle \Psi_{\mathrm{f}} | \vec{A} \cdot \vec{P} | \Psi_{\mathrm{np}_x} \rangle|^2 = 0$, because both the final state of photoelectron wave function Ψ_{f} and the term $\vec{A} \cdot \vec{P}$ lying in the mirror plane k_y–k_z are even, but Ψ_{npx} is odd relative to the mirror plane k_y–k_z. However, the presence of TEF along x axis may generate the hybridization between s electron orbital and p_x electron orbital, which enables the term $|\langle \Psi_{\mathrm{f}} | \vec{A} \cdot \vec{P} | \Psi'_{\mathrm{np}_x} \rangle|^2 > 0$ to contribute to the ARPES intensity along k_y axis. In the related experiments, one may find that when the incident photons having s polarization are scattered in the k_x–k_z plane, the corresponding ARPES intensity along k_y axis may be more or less stronger than that along k_x axis.

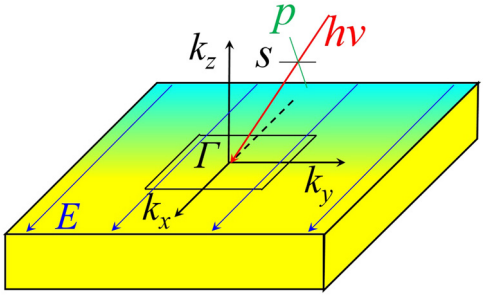

Figure 7: Schematic diagram of a beam of photons (denoted by red line) with s polarization (photon electric field perpendicular to the scattering plane k_x–k_z) or p polarization (photon electric field lying in the scattering plane k_x–k_z) radiating at a metal surface with tetragonal symmetry. The TEF indicated by blue arrows is along k_x direction.

2.2.4 Effect on the scanning tunneling microscope or spectroscopy (STM/STS)

The altered Fermi level and the correlated TEF may have a non-negligible influence on the STM/STS. And the tunneling current may be changed by the induced variations in the density of state (DOS) and work function. For a region with altered Fermi level at a metal surface, a tunneling current may appear when an electrical bias voltage V_{bias} would be applied at low temperatures. The current could be written as follows [37,38]:

$$I \approx \frac{4\pi e}{\hbar} |M|^2 N_{\mathrm{t}}(E_{\mathrm{F0}}) \int \mathrm{d}\varepsilon N_{\mathrm{s}}(\varepsilon) [f(\varepsilon - eV_Z) - f(\varepsilon + eV_{\mathrm{bias}} - eV_Z)], \tag{40}$$

where M is the tunneling matrix element, $N_{\mathrm{t}}(E_{\mathrm{F0}})$ is the DOS at the Fermi level E_{F0} of the tip, $N_{\mathrm{s}}(\varepsilon)$ is the energy ε dependent DOS of the sample surface confronting the tip, and f is the Fermi-Dirac distribution function. The local DOS of the sample may be a slowly varying function, so Eq. (40) could be simplified to

$$I \approx \frac{4\pi e^2 V_{\mathrm{bias}}}{\hbar} |M|^2 N_{\mathrm{t}}(E_{\mathrm{F0}}) N_{\mathrm{S}}(E_{\mathrm{F}} + eV_Z), \tag{41}$$

where E_{F} is the altered Fermi level of the region, and V_{Z} is the electric potential difference between this region and surrounding regions with initial Fermi level E_{F0} as shown in Figure 8, and it is $E_{\mathrm{F}} + eV_{\mathrm{Z}} = E_{\mathrm{F0}}$. Based on Eq. (41), one may find that for the region with altered Fermi level, the tunneling current may be determined by its local DOS at the corresponding energy level ($E_{\mathrm{F}} + eV_{\mathrm{Z}}$) instead of its local DOS at the Fermi level E_{F}.

On the other hand, owing to the alteration in Fermi level, the work function of the electron in this region may be changed

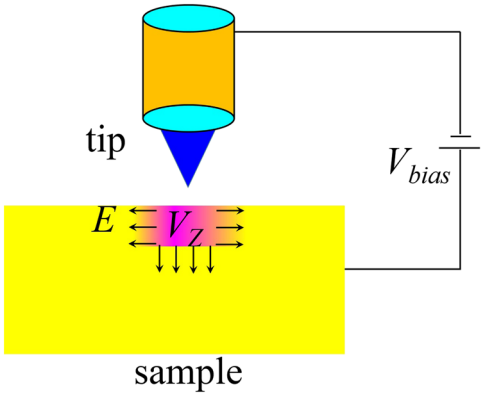

Figure 8: A bias voltage V_{bias} between tip of STM and metal surface with the up-shifted Fermi level colored by magenta. The up-shifted Fermi level may make this region possess a positive electric potential V_Z and the surrounding electric field is shown by black arrows.

$$\phi_s = \phi_{s0} + eV_Z, \tag{42}$$

where ϕ_{s0} denotes the work function of the metal surface with pristine Fermi level, and ϕ_s *is* the work function of the metal surface with altered Fermi level. The variations in the work function may further lift the tunneling current by changing the key parameter, *i.e.*, inverse decay length, because the tunneling current is $I \propto e^{-2\kappa d}$, where κ is the inverse decay length and d is the distance between tip and sample surface [39]. The modified inverse decay length may be given by [40,41]

$$\kappa = \sqrt{\frac{2m_e}{\hbar^2}\left(\frac{\phi_t + \phi_{s0} + eV_Z}{2} - W + \frac{e|V_{bias}|}{2}\right)}, \tag{43}$$

where W is the energy of the state relative to the Fermi level E_F. As is shown in this equation, the regions of metal surface with up-shifted Fermi level would be expected to yield an enhanced tunneling current and *vice versa*. These regions may be detected by the constant height mode of operation for STM.

2.2.5 Surface transport and segregation

Analogous to the case of metals [42], the TEF at the surface of metallic terminal solid solution (MTSS) may also cause a composition segregation. For simplicity, the two-component MTSS could be investigated as an example. For the minority atoms at MTSS surface, their diffusion flux could be given by the famous Fick's law [43].

$$j_0 = -D\nabla n(\vec{r}, t), \tag{44}$$

where $n(r, t)$ is the position r and time t dependent minority atom concentration, and D is the diffusion constant at the surface. Based on Einstein diffusion relation, the diffusion constant equals to $D = uk_BT$, where k_B is the Boltzmann constant, T is the temperature, and u is the mobility of minority atom at the surface.

In view of the possible TEF at the surfaces, the field-induced another transport mechanism may play an important role in the evolution processes of the surface composition. Despite many factors that enable the Fermi level to shift and thereby induce a related electric field, only the electric field originating from the inhomogeneous strain is considered. By employing Yuheng Zhang equation, the electric field generated by the non-uniform strain at a surface normal to z axis may be

$$\vec{E}_1 = \frac{1}{e}\frac{dE_F}{d\xi_{zi}}\nabla\xi_{zi}, \tag{45}$$

where ξ_{zi} $(i = x, y, z)$ is the strain components at the surface normal to z axis and the subscript indices obey Einstein summation convention, and $dE_F/d\xi_{zi}$ denotes the mechanical-electric coupling of the MTSS. According to Teorell's theory [44], the electric field would result in a correlated drift term and it is

$$j_1 = n(\vec{r}, t)u\frac{Q}{e}\frac{dE_F}{d\xi_{zi}}\nabla\xi_{zi}, \tag{46}$$

where Q denotes the net charges carried by a minority atom due to the electronegativity differences between the minority atoms and the majority atoms.

In terms of Eq. (1), the inhomogeneous distribution of minority atoms at the MTSS surface may also give rise to a tangential electric field along the surface and it may be

$$\vec{E}_2 = \frac{1}{e}\frac{dE_F}{dn}\nabla n(\vec{r}, t), \tag{47}$$

where e is the electron charge, and E_F is the minority atom concentration dependence of Fermi level. Likewise, this field may create another drift flux of the minority atoms and it could be given by

$$j_2 = n(\vec{r}, t)u\frac{Q}{e}\frac{dE_F}{dn}\nabla n(\vec{r}, t). \tag{48}$$

The total transport flux of the minority atoms at the TMSS surface may be the summation of the diffusion term and the two drift terms.

$$j_t = -D[1 - \alpha n(\vec{r}, t)]\nabla n(\vec{r}, t) + n(\vec{r}, t)\frac{D}{k_BT}\frac{Q}{e}\frac{dE_F}{d\xi_{zi}}\nabla\xi_{zi}, \tag{49}$$

where the parameter is $\alpha = Q(dE_F/dn)/ek_BT$. When the equilibrium state is approached, the total transport flux of the atoms at the MTSS surface may be rigorously zero. So, the distribution of the minority atoms at the MTSS surface could be obtained analytically

$$n(\vec{r}) = -\frac{1}{\alpha}\text{ProductLog}\left[-\alpha n(\vec{r}_0)\exp\left(\frac{Q\Delta E_F}{ek_BT} - \alpha n(\vec{r}_0)\right)\right], \quad (50)$$

where the mathematical function is defined as ProductLog $(\lambda e^{\lambda}) = \lambda$, the Fermi level difference ΔE_F stemming from strains is $\Delta E_F = E_F(r) - E_F(r_0)$. It can be seen that the existence of a TEF at MTSS surface may induce the surface composition segregation, which may further influence the physical properties and chemical properties of the surface. If the magnitude of the product is very small $|\alpha n(r)| \ll 1$, this equation could be simplified to

$$n(\vec{r}) \approx n(r_0)e^{Q\Delta E_F/ek_BT}, \quad (51)$$

It may indicate that the composition distribution at the MTSS surface may be controlled by the temperature T, the electronegativity difference, and the shifted Fermi level caused by the strains. At high temperatures, the composition distribution at the surface may be much more uniform than that at low temperatures. A smaller electronegativity difference between the minority atoms and the majority atoms may lead to a relatively uniform composition distribution and *vice versa*. In general, the continuous solid solutions [45] listed in Table 1 may exhibit a much more uniform composition distribution, whereas the discontinuous solid solutions especially those with small solid solubility usually display serious composition segregation. This may be consistent with investigations on the surface segregation of bimetallic nanoparticles [46]. Another important factor is the Fermi level difference that usually originates from the popular strains at the MTSS surface because of the residual stresses and various types of defects such as dislocations. Here a preliminary estimation may be helpful and necessary. The residual stresses could usually reach several hundred MPa [13,14,32,33], so the residual strain may be several thousands. For most MTSS, the mechanical-electric coupling strength may be in the range of 1–10 eV, thereby creating a Fermi level difference ΔE_F in the range of 5–50 meV at the surfaces, which agrees with the experimentally observed magnitude of the surface potential variations [5–7]. If the net charge carried by a minority atom is an electron charge, the room-temperature-composition segregation ratio at the surface might reach 1.2–7 according to Eq. (51), which may be in qualitative accordance with the segregation ratio induced by the enrichment of Pt atoms at edges and corners of the nanoparticle surfaces [47,48]. In another respect, the more commonly observed is the radial strain reaching ~1% for many nanoparticles, so a Fermi level difference ΔE_F of 10–100 meV may be yielded along the radius of the nanoparticles. If the net charge carried by a minority atom is also an electron charge, the room-temperature segregation ratio estimated by Eq. (51) may be in the range of 1.5–50, which is consistent with the experimental investigations on segregation ratio in bimetallic nanoparticles [46–49]. The above estimations may prove rationality of Eq. (51) in spite of their roughness. To get much more precise segregation ratio by using Eq. (51), one should obtain more accurate parameters Q and ΔE_F.

Table 1: Binary continuous solid solutions according to Okamoto *et al*. [45]

The groups in periodic table	Continuous solid solutions ($0 \le x \le 1$)			
Main group 1	Cs_xRb_{1-x}	K_xRb_{1-x}		
Main group 4	Ge_xSi_{1-x}			
Main group 5	Bi_xSb_{1-x}			
Main group 6	Se_xTe_{1-x}			
Subgroups 5, 6	Cr_xV_{1-x}	Mo_xTa_{1-x}	Mo_xV_{1-x}	Nb_xTa_{1-x}
Subgroups 5, 6	Mo_xW_{1-x}	Nb_xV_{1-x}	Nb_xW_{1-x}	Mo_xNb_{1-x}
Subgroups 5, 6	Ta_xW_{1-x}	V_xW_{1-x}		
Subgroups 7, 8	Os_xRu_{1-x}	Os_xRe_{1-x}	Re_xRu_{1-x}	
Subgroups 10,11	Ag_xPd_{1-x}	Ni_xPd_{1-x}	Ag_xAu_{1-x}	

2.2.6 Effect on field emission

Field emission is an important technique and has been applied in numerous areas such as the field emission microscopy. Under an externally applied strong electric field shown in Figure 9(a), the electrons in a cold metal can tunnel into vacuum and form an electrical current. According to the famous field emission model proposed by Fowler and Nordheim [50], the current is

$$I = \frac{4\sqrt{\varepsilon_F\phi}}{(\varepsilon_F + \phi)}\frac{e^3E}{16\pi^2\hbar\phi}\exp\left(-\frac{4\sqrt{2m_e}\phi^{3/2}}{3\hbar eE}\right), \quad (52)$$

where ε_F is the Fermi energy, *i.e*., the largest kinetic energy for free electrons in a metal at zero temperature, ϕ is the work function, E is the applied intense electric field at the metal surface, and e presents the electron charge.

The field emission process of a cold metal may be affected by the existence of TEF at the metal surface

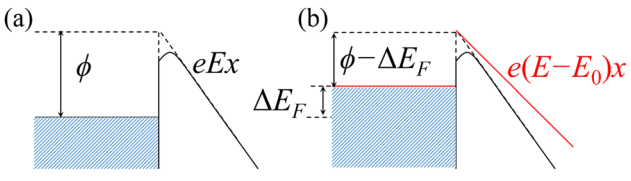

Figure 9: Sketch of field emission for a metal. (a) electron emission for the metal with a work function ϕ under an intense field E at the metal surface; and (b) electron emission for the region with a shifted Fermi level by the amount ΔE_F and the related electric field is changed to be E–E_0 where E_0 results from the shifted Fermi level.

from two respects. As displayed by Figure 9(b), one is the shifted Fermi level whose variations may correspond to the changes in work function at the low temperatures. The other may be the weak modifications on the intense electric field at the metal surface. The updated electrical current due to field emission may be given by

$$I' = \frac{4\sqrt{\varepsilon_F'(\phi - \Delta E_F)}}{[\varepsilon_F' + (\phi - \Delta E_F)]} \frac{e^3(E - E_0)}{16\pi^2\hbar\phi} \exp\left\{ -\frac{4\sqrt{2m_e}(\phi - \Delta E_F)^{3/2}}{3\hbar e(E - E_0)} \right\}, \quad (53)$$

where ε_F' is the shifted Fermi energy, ΔE_F is the lifted amount of Fermi level, and E_0 denotes the electric field arising from the shifted Fermi level and it may be much weaker than the applied intense field.

As shown by this equation, the up-lifted Fermi level region at the metal surface may generate a larger field emission current, because the related work function may be weakened. Whereas the down-lifted Fermi level region may cause a smaller field emission current. For the material surfaces such as the nanoparticle surfaces, the experiments and simulations indicated that a smaller radius of curvature can usually yield a larger local strain [51–57]. According to the mechanical-electric coupling in metals, *i.e.*, Yuheng Zhang effect, the noticeable local strain may lead to an apparent shift in the Fermi level. Therefore, it could be inferred that both the intense field and up-shifted Fermi level due to notable local strain play an important role in the field emission of a sharp tip with a radius of curvature in nanoscale.

2.2.7 Micro-earth

The experimental and theoretical investigations indicated that a dramatic and widespread strain gradient exists along the radius of nanoparticles [51–57]. According to the Yuheng Zhang effect and Yuheng Zhang equation [9,10], this strain gradient in the nanoparticles may give rise to a corresponding electric field along their radius, and it could be given by ref. [11]

$$\vec{E}_n = \frac{\partial E_F}{e\partial\xi_{ij}}\nabla\xi_{ij}, \quad (54)$$

where ξ_{ij} is the strain components. For a nanoparticle with a radius of several nanometers, the internal radial electric field may approach a magnitude ~10^8 V/m. Hence, a noticeable charge separation may appear in the nanoparticle and a larger number of charges could accumulate at the nanoparticle surfaces. For simplicity, this electric field is assumed to be a constant and the charge density distribution within the metal nanoparticles may be approximated as that in the core of the earth [58].

$$\rho(r) = 2D/r - D\delta(r - r_0), \quad (55)$$

where r_0 is the radius of the metal nanoparticle, $\rho(r)$ is the radius dependence of charge density, and the parameter D is the electric displacement $D = \varepsilon_0\varepsilon E_n$ and its magnitude may reach a value 10 C/m^2 for some metal nanoparticles. Analogous to the possible creation of the earth's geomagnetic field [58], the fast rotation of such a metal nanoparticle from west to east (the same rotational direction as the earth) will generate a correlated magnetic field which may be described in cylindrical coordinate system as shown in Figure 10.

$$\begin{aligned} B_r &= -\pi\frac{\mu_0 D}{2T}\frac{r_0^4}{R^3}\sin 2\psi \quad (R > r_0) \\ B_\varphi &= 0 \\ B_z &= -\frac{\pi}{3}\frac{\mu_0 D}{2T}\frac{r_0^4}{R^3}(1 + 3\cos 2\psi) \quad (R > r_0). \end{aligned} \quad (56)$$

where R is the distance from center of the metal nanoparticle, T is the period of rotation, μ_0 is the magnetic susceptibility outside the nanoparticle, ψ is the polar angle from positive z-axis, and φ is the azimuthal angle in the x–y plane from the x-axis.

These equations display that the yielded magnetic field is a magnetic dipole field. For a metal nanoparticle with an average radius of 2 nm, if the period of its fast rotation could be 1 ps, a magnetic dipole field may be created around the nanoparticle and the field strength at the equator may reach ~200 Gauss. The electric field along the radius of the metal nanoparticles may be assumed to be a constant, but the actual electric displacement may not be a constant and varies with the position. So, the above

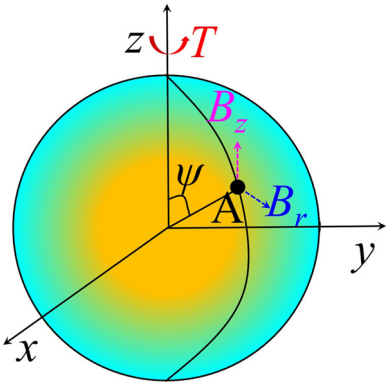

Figure 10: Schematic diagram of a magnetic dipole field yielded by fast rotation of a metal nanoparticle.

calculations could mainly predict the mechanism of magnetic field yielded by the fast rotation of a metal nanoparticle and a more precise determination of the magnetic field would still depend on a more precise position dependence of electric displacement vector.

In spite of the remarkable size difference between the metal nanoparticle and the earth, the fast rotation of a metal nanoparticle may be very like the earth considering the following points. First, a notable charge separation exists along the radius for both the metal nanoparticle and the metallic core of the earth due to Yuheng Zhang effect. Second, according to the possible mechanism of the earth's geomagnetic field [58], the fast rotation of both the metal nanoparticle and the earth could generate a magnetic dipole field. Taking these similarities into account, the rotating metal nanoparticle may be named as "micro-earth." How can people give birth to such a fast rotated micro-earth? A possible method might employ the incidence of photons with an angular momentum. The effective transfer of the angular momentum of photons to a nanoparticle may enable it to rotate rapidly and yield a micro-earth. In the future, the micro-earth may be utilized in some important areas such as micro-detection.

2.2.8 Adsorption of molecules at nanoparticle surface

As indicated in Section 2.2.7, the popular strain gradient in the nanoparticles usually generate a noticeable charge separation and the charges may agglomerate at surfaces especially the sharp edges and the shared corners as shown in Figure 11. As a result, an intense electrostatic field may be created in the vicinity of the nanoparticle surface. The field may sensitively depend on the position and decay rapidly with the distance away from the surface. In general, the spatial distribution of the electrostatic field may exhibit the following properties:

$$\begin{aligned} E(r) &\propto \frac{1}{r^2} \quad (r < l_0); \\ E(r) &\propto \frac{1}{r^3} \quad (l_0 < r < 2R_0); \\ E(r) &\propto \frac{1}{r^4} \quad (2R_0 < r); \end{aligned} \tag{57}$$

where r is the distance away from the nanoparticle surface, l_0 denotes the surface strain relaxation length and is usually the length of several atomic layers ~1 nm [53,57,59], and R_0 is the radius of the nanoparticle. The electrostatic field may approach a magnitude ~10^8 V/m for the molecules adsorbed on the surface and even reach ~10^9 V/m near the sharp edges and shared corners. The existence

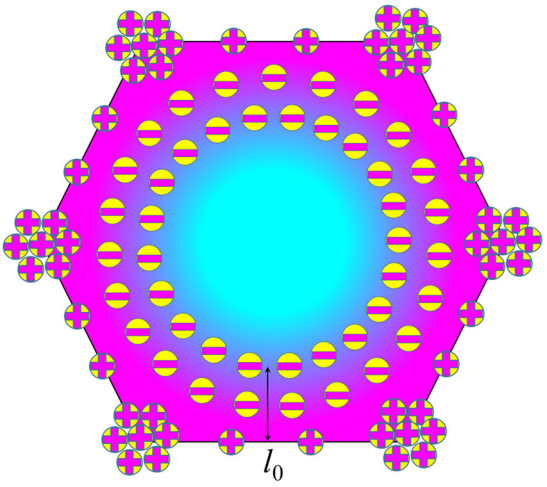

Figure 11: Sketch of a cutaway drawing for a nanoparticle with charge separation. The strain (magenta zone and the strain relaxation length l_0) due to surface relaxation may exist along the radius and could cause the related remarkable charge separation. The net charges at the surface may mainly be distributed at the sharp edges and shared corners.

of an intense electrostatic field affecting the thermodynamic behaviors of gas adsorption heavily can be expected. For the molecule system, the Gibbs energy change is as follows:

$$\mathrm{d}G = -S\mathrm{d}T + V\mathrm{d}p - Vn\langle p_\mathrm{e}\rangle \mathrm{d}E, \tag{58}$$

where G is the Gibbs energy of the molecule system, $n = N/V$ is the concentration of molecules, V is the volume per mole molecules, N is the Avogadro constant, p is the pressure of the gas molecules, E is the electric field, p_e denotes the intrinsic dipole moment of an individual molecule, and $\langle p_\mathrm{e}\rangle$ is the thermal average value and it could be given by

$$\frac{\langle p_\mathrm{e}\rangle E(\vec{r})}{k_\mathrm{B}T} = \frac{p_\mathrm{e}E(\vec{r})}{k_\mathrm{B}T}\coth\left[\frac{p_\mathrm{e}E(\vec{r})}{k_\mathrm{B}T}\right] - 1 + \frac{\alpha_\mathrm{e}E^2}{2k_\mathrm{B}T}, \tag{59}$$

where $E(r)$ is the position-dependent electric field, the parameter k_B is the Boltzmann constant, T is the temperature, and α_e stands for the electric polarizability of a molecule. Generally speaking, the polarizability α_e sometimes exhibits anisotropy and thus may be described better by a matrix. But it could be assumed to be a constant for simplicity in the following discussions.

When the neutral molecule system reaches thermal equilibrium, the spatial gradient of Gibbs energy must be zero and the equilibrium equation is as follows:

$$\nabla p - n\langle p_\mathrm{e}\rangle \nabla E(\vec{r}) = 0. \tag{60}$$

In the above calculations, the field effect on the electric dipole–dipole interaction is ignored for simplicity. Using Van der Waals equation [60,61] for 1 mole gas molecules,

$$\left(p + \frac{a}{V^2}\right)(V - b) = RT,$$

where a is a parameter arising from the attractive interaction between molecules [60,61], b is the parameter due to the finite volume of a molecule, and R is the gas constant.

Substitute Van der Waals equation in Eq. (60),

$$\left[\frac{k_B T}{n(1 - nb/N)^2} - \frac{2a}{N^2}\right]\nabla n = \langle p_e\rangle \nabla E(\vec{r}). \tag{61}$$

Its analytical solution may be

$$\begin{aligned}&\left(1 - \frac{nb}{N}\right)^{-1} + \ln n - \ln\left(1 - \frac{nb}{N}\right) - \frac{2an}{NRT} - \frac{\langle p_e\rangle E(\vec{r})}{k_B T}\\ &= \left(1 - \frac{n_0 b}{N}\right)^{-1} + \ln n_0 - \ln\left(1 - \frac{n_0 b}{N}\right) - \frac{2an_0}{NRT},\end{aligned} \tag{62}$$

where n_0 is the concentration of molecules far away from the nanoparticles. In most cases, the relation $nb/N \ll 1$ holds, meaning that the volume of molecules in gas state may be far larger than that for the same number of molecules in liquid state. Thus, the equation may be approximated as

$$\begin{aligned}&\ln n - \left(\frac{2a}{NRT} - \frac{2b}{N}\right)n - \frac{\langle p_e\rangle E(\vec{r})}{k_B T}\\ &\approx \ln n_0 - \left(\frac{2a}{NRT} - \frac{2b}{N}\right)n_0.\end{aligned} \tag{63}$$

Let the important parameter λ be

$$\lambda = \frac{2a}{NRT} - \frac{2b}{N}. \tag{64}$$

The above equation could be written as follows:

$$ne^{-\lambda n} = n_0 e^{-\lambda n_0} e^{\langle p_e\rangle E(\vec{r})/k_B T}. \tag{65}$$

Its precise solution could be given by

$$n = \frac{-1}{\lambda}\text{ProductLog}(-\lambda n_0 e^{-\lambda n_0} e^{\langle p_e\rangle E(\vec{r})/k_B T}), \tag{66}$$

where the function is ProductLog($x \cdot e^x$) = x. It indicates that the concentration of the adsorbed molecules at the nanoparticle surface may rely on several important factors such as the temperature, the magnitude of electric field, and the electric dipole of a molecule. The temperature has an important effect and the concentration increases as the temperatures drops. A more intense electric field at the nanoparticle surface would lead to a larger concentration. In addition, a bigger electric dipole of the molecule may also result in a larger concentration and *vice versa*. When the concentration of the adsorbed molecules at the nanoparticle surface reaches the saturation vapor concentration, the liquefaction may happen.

Considering the possible liquefaction in the vicinity of the nanoparticle surface, the whole adsorption around the nanoparticles may be contributed by two typical regions. The first is the region where the electric field is weak and decays rapidly with distance from the nanoparticle surface, thereby corresponding to the region full of molecules in the gaseous state.

In most situations, the relation may be valid $|\lambda n_s| \ll 1$ where n_s is the saturation vapor concentration, so Eq. (66) could be simplified to

$$n \approx \frac{n_0 e^{\langle p_e\rangle E(\vec{r})/k_B T}}{1 - \lambda n_0 (e^{\langle p_e\rangle E(\vec{r})/k_B T} - 1)}. \tag{67}$$

The concentration of the adsorbed gas molecules near nanoparticle surface may be approximately proportional to the concentration n_0 far away from the nanoparticles. The approximate relation between the gas pressure and the concentration of the gaseous molecules could be taken as $n_0 \approx p_0/k_B T$, where p_0 is the gas pressure. In reality, this approximation is the equation of state for the ideal gas. Thus, the adsorbed mass of the gaseous molecules could be given by

$$M_a \approx \frac{mp_0}{k_B T}\int e^{\langle p_e\rangle E(\vec{r})/k_B T} - 1 \mathrm{d}V, \tag{68}$$

where m is the mass of an individual molecule, M_a is the total mass of the adsorbed molecules. It shows that the mass of the adsorbed molecule may be proportional to the gas pressure and the proportionality constant may become large at low temperatures, which is usually observed in experiments when the gas pressure is very low [62]. At relatively high temperatures, the relations $p_e E(\vec{r})/k_B T \ll 1$ and $\alpha_e E^2(\vec{r})/k_B T \ll 1$ may be fulfilled so that Eq. (59) could be approximated to be $\langle p_e\rangle E(\vec{r})/kT \approx \frac{\left[\frac{p_e E(\vec{r})}{kT}\right]^2}{3} + \alpha_e E^2(\vec{r})/2k_B T$. As a result, the adsorbed mass given by Eq. (68) could be written as follows:

$$M_a \approx \frac{mp_0}{k_B T}\left[\frac{p_e^2}{3(k_B T)^2} + \frac{\alpha_e}{2k_B T}\right]\int E^2(\vec{r})\mathrm{d}V. \tag{69}$$

As is demonstrated, the adsorbed mass of the gaseous molecules may be proportional to the electrostatic energy around the nanoparticles. And the adsorbed quantity would be larger for the molecules with a bigger dipole moment p_e and a bigger polarizability α_e.

In another case $\lambda n_s \sim 1$, the relation between the concentration n under the electric field and the concentration n_0 may exhibit a concave hyperbolic curve given in Figure 11. This case may be rarely encountered in experiments because it requires the condition $\lambda n_s \sim 1$ that most kinds of gas molecules cannot satisfy.

Interestingly, if the parameter λ displays a negative value and the relation $-\lambda n_s \sim 1$ exists, the concentration n_0 versus the concentration n may present a convex hyperbolic curve as shown in Figure 12. Considering the required negative value of the parameter λ, it may also be difficult for this case to be observed in experiments.

The second region is the liquefaction region where the molecule concentration reaches the value of liquid state, *i.e.*, $n = n_l$, and its volume could be denoted as V_l. At the boundaries between the liquefaction region and gaseous region, the concentration of the gas molecules may reach the saturation vapor pressure p_s which corresponds to saturation vapor concentration n_s,

$$n_s = \frac{-1}{\lambda}\text{ProductLog}(-\lambda n_0 e^{-\lambda n_0} e^{\langle p_e\rangle E(\vec{r})/k_B T}). \tag{70}$$

Combining Eqs. (59) and (70), a corresponding saturated electric field (SEF) may be uncovered.

$$\begin{aligned}&\frac{p_e E_s}{k_B T}\coth\left(\frac{p_e E_s}{k_B T}\right) - 1 + \frac{\alpha_e E_s^2}{2k_B T} \\ &= (\ln n_s - \ln n_0 + \lambda n_0 - \lambda n_s).\end{aligned} \tag{71}$$

The existence of SEF means that the regions with electric field higher than SEF will accommodate the condensed molecules and form the liquefaction zones $V_l = V(E \geq E_s)$. For the non-polar molecules whose net dipole moment is zero, the SEF could be

$$E_s = \sqrt{\frac{2k_B T}{\alpha_e}}\left(\ln\frac{n_s}{n_0} + \lambda n_0 - \lambda n_s\right)^{1/2}. \tag{72}$$

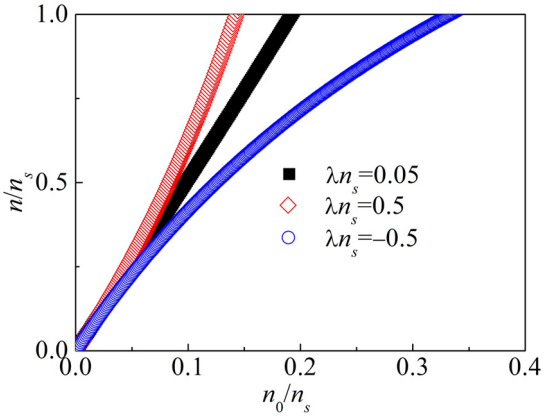

Figure 12: The reduced concentration n/n_s (n_s is the saturation vapor concentration) of adsorbed gas molecules in the vicinity of nanoparticle surface *vs* the reduced concentration n_0/n_s far away from the nanoparticles. The black squares denote the curve with parameter $\lambda n_s = 0.05$, the red diamonds denote the curve with parameter $\lambda n_s = 0.5$, and the blue circles denote the curve with parameter $\lambda n_s = -0.5$.

For polar molecules, the approximate expression of SEF in some situations could be

$$E_s \approx \begin{cases} \dfrac{\sqrt{6}\,k_B T}{\sqrt{2p_e^2 + 3\alpha_e k_B T}}\left(\ln\dfrac{n_s}{n_0} + \lambda n_0 - \lambda n_s\right)^{1/2}; & \dfrac{p_e E}{k_B T} \ll 1 \\ \dfrac{p_e}{\alpha_e}\left[\sqrt{1 + 2\alpha_e k_B T\left(1 + \ln\dfrac{n_s}{n_0} + \lambda n_0 - \lambda n_s\right)/p_e^2} - 1\right]; & \\ \dfrac{p_e E}{k_B T} \gg 1. & \end{cases} \tag{73}$$

In general, SEF decreases as the temperature drops, suggesting a growing liquefaction volume of the absorption molecules as the temperature is decreasing. In another respect, a bigger dipole moment of the molecules corresponds to a smaller SEF, which usually leads to a larger liquefaction region near the nanoparticle surfaces.

As a result, the total mass M_a of the adsorbed molecules in the vicinity of nanoparticles could be obtained as follows:

$$M_a = mV_l(n_l - n_0) + m\int_{E\leq E_s}(n - n_0)\mathrm{d}V, \tag{74}$$

where V_l is the liquefaction volume at the nanoparticle surface, and n_l is the concentration of molecules in the liquid state. It may be difficult to accurately determine the amount of adsorbed gas molecules due to the absence of the detailed spatial dependence of electrostatic field near the nanoparticle surfaces. But the general law of absorption could be revealed. As the temperature decreases, the SEF decreases but the adsorbed concentration of molecules usually increases, both of which would inevitably bring a larger amount of adsorption. Moreover, as is indicated previously, a smaller nanoparticle usually generates a stronger electric field that may lead to a larger adsorption concentration based on Eq. (67). As a result, a larger number of molecules could be adsorbed by the same mass of nanoparticles.

For the calculations in this section, to uncover the electrostatic field effect on the adsorption, only the polarization energy and the induction energy was taken into account, but the important dispersion energy and the electrostatic field effect on the interaction between gas molecules were ignored for simplicity. In the future, a whole model considering all the energies may need to be constructed to understand the complex adsorption behaviors of nanoparticles.

2.2.9 Modification on the molecular orbital of adsorbed molecules

The electrostatic field near the nanoparticle surface may give rise to some modifications on the molecular structure of the adsorbed molecules. To show this effect, the simplest

Hamiltonian for an electron with two-orbital basis is taken for clarity in physics,

$$H_0 = E_a|a\rangle\langle a| + E_b|b\rangle\langle b| + V|a\rangle\langle b| + V^{\dagger}|b\rangle\langle a|, \quad (75)$$

where E_a and E_b are the eigenenergy for the two electron orbitals, $|a\rangle$ and $|b\rangle$ are the Dirac bras for the two electron orbitals, and V is the orbital overlap energy. The electrostatic field may induce other off-diagonal matrix elements such as $\langle e\vec{E}\cdot\vec{r}\rangle_{ab}|a\rangle\langle b|$ and $\langle e\vec{E}\cdot\vec{r}\rangle_{ba}|b\rangle\langle a|$. Here their related diagonal matrix elements are ignored, because they may be much smaller than the eigenenergy E_a and E_b for the two electron orbitals. The total Hamiltonian is

$$\begin{aligned} H = {} & E_a|a\rangle\langle a| + E_b|b\rangle\langle b| + V|a\rangle\langle b| + V^{\dagger}|b\rangle\langle a| \\ & + \langle e\vec{E}\cdot\vec{r}\rangle_{ab}|a\rangle\langle b| + \langle e\vec{E}\cdot\vec{r}\rangle_{ba}|b\rangle\langle a|, \end{aligned} \quad (76)$$

where the terms are $\langle\rangle_{ab} = \langle a||b\rangle$ and $\langle\rangle_{ba} = \langle b||a\rangle$. For the covalent bonds where the relation $|E_a - E_b| \ll |V|$ exists, the resultant solution for the total Hamiltonian can be obtained.

$$\begin{aligned} E_{\pm} \approx {} & \frac{E_a + E_b}{2} \pm |V + \langle e\vec{E}\cdot\vec{r}\rangle_{ab}|\Bigg[1 \\ & + \frac{(E_a - E_b)^2}{8|V + \langle e\vec{E}\cdot\vec{r}\rangle_{ab}|^2}\Bigg]. \end{aligned} \quad (77)$$

As is seen clearly, the covalent bond strength may be modified by the electrostatic field, and a larger field usually causes a more notable modification. A field with magnitude ~10^9 V/m may lead to an energy shift ~0.1 eV. Hence, the electric structure of molecules physically adsorbed at the nanoparticle surfaces may often be altered to some extent. And it may bring some shifts for the related fluorescence, infrared spectroscopy, Raman spectroscopy, and nuclear magnetic resonance spectroscopy of the adsorbed molecules. The spectrum shift of the adsorbed molecules may vary with distance and could approach several percent. Besides, the electrostatic field in the vicinity of nanoparticles may display a remarkable electric quadrupole field which may influence selection rules for the related spectrum.

2.2.10 Quenching of fluorescence

Because of the charge separation and accumulation at the metallic nanoparticle surface shown in Figure 11, an ultrastrong electric field may be yielded and applied to the nearby molecules. Thus, a related electrostatic dipole may be generated in the molecule, and a strong static dipole–dipole interaction (SDD) may appear between the metallic nanoparticles and the adjacent molecules. The Hamiltonian could be written as follows:

$$H_{\mathrm{dd}} \approx \frac{1}{4\pi\varepsilon_0}\sum_i\left[\frac{\vec{P}_{\mathrm{e}}\cdot\vec{p}_i(\vec{r}_i)}{|\vec{r}_i|^3} - \frac{3(\vec{P}_{\mathrm{e}}\cdot\vec{r}_i)(\vec{p}_i(\vec{r}_i)\cdot\vec{r}_i)}{|\vec{r}_i|^5}\right], \quad (78)$$

where P_{e} is the near-field electric dipole moment at the nanoparticle and it may be proportional to the internal electric field along the radius in the nanoparticle $P_{\mathrm{e}} \propto \alpha_{\mathrm{n}}(0)E$, α_{n} is the electrostatic polarizability of nanoparticle, $p_i(r_i)$ denotes the electric dipole moment of a molecule at position r_i and it may sensitively depend on the local electrostatic field $E(r_i)$ exerted by the adjacent nanoparticle, and ε_0 is the vacuum permittivity.

This SDD may exhibit several typical properties. First, it may be a near-field interaction. It can be very strong within a small scale ($r \sim l_0$) and the strength may be $H_{\mathrm{dd}} \propto \alpha_{\mathrm{n}}(0)E_{\mathrm{n}}\alpha_{\mathrm{m}}(0)E(r_i)$, where $\alpha_{\mathrm{m}}(0)$ represents the electrostatic polarizability of the molecules at the position r_i. Second, it sensitively relies on the electrostatic polarizability of nanoparticle α_{n}, and a bigger polarizability can not only give birth to a larger near-field electric dipole moment at the nanoparticle but also cause a much more intense electrostatic field around the nanoparticle. The static polarizability of metals may be large and could be proportional to the square of the phenomenological relaxation time τ of electrons $\alpha_{\mathrm{n}}(0) \propto (\omega_{\mathrm{p}}\tau)^2$ [5,17], where ω_{p} is the plasma frequency. In addition, the electron relaxation time τ is usually proportional to the direct current electrical conductivity $\sigma(0)$ so that the relation exists $\alpha_{\mathrm{n}}(0)\propto[\sigma(0)]^2$. Considering that the electrostatic field $E(r_i)$ around the metallic nanoparticle may linearly depend on the amount of separated net charges in the nanoparticle, the strength of SDD interaction may be proportional to the square of static polarizability $H_{\mathrm{dd}} \propto [\alpha_{\mathrm{n}}(0)]^2$. Therefore, the strength of SDD interaction may be $H_{\mathrm{dd}} \propto [\sigma(0)]^4$. It means that the metallic nanoparticles especially those with much higher direct current electrical conductivity $\sigma(0)$ may usually result in a stronger SDD interaction. Third, the SDD interaction may decay very quickly with the increasing distance, as may be ascribed to two main factors. One is the fast attenuation of the local electrostatic field $E(r_i)$ applied on the molecule, which may reduce the electric dipole moment $p_i(r_i)$ of a molecule. The other is the natural attenuation of the SDD interaction with distance as shown by the above equation. Hence, the distance dependence of the SDD is as follows

$$\begin{aligned} H_{\mathrm{dd}} &\propto \frac{1}{r^5} \quad (r < l_0); \\ H_{\mathrm{dd}} &\propto \frac{1}{r^6} \quad (l_0 < r < 2R_0); \\ H_{\mathrm{dd}} &\propto \frac{1}{r^7} \quad (2R_0 < r); \end{aligned} \quad (79)$$

This near-field SDD interaction may be very strong and play a key role for the quenching of fluorescence.

The related quantum mechanism may be illustrated in Figure 13. When a beam of laser is incident on the molecules, the electrons in the molecular ground state would hop to excited states in terms of absorbing energy-matched photons shown in Figure 13(a). The related quantum transition is a one-photon process and can be described well by Fermi golden rule [17].

$$W_{\mathrm{f}\leftarrow\mathrm{i}} = \frac{2\pi}{\hbar}\left|\langle\psi_{\mathrm{e}}|\frac{eE_0}{m_{\mathrm{e}}\omega}e^{i\vec{k}\cdot\vec{r}}\vec{e}\cdot\vec{p}|\psi_{\mathrm{g}}\rangle\right|^2 \delta(\varepsilon_{\mathrm{me}} - \varepsilon_{\mathrm{mg}} - \hbar\omega), \tag{80}$$

where $W_{\mathrm{f}\leftarrow\mathrm{i}}$ is the quantum transition rate from the ground state $|\psi_{\mathrm{g}}\rangle$ to the excited state $|\psi_{\mathrm{e}}\rangle$, $\vec{e}$ is the polarization unit vector of incident laser beam, E_0 is the magnitude of electric field of the laser, $\vec{p}$ is the momentum operator, $\varepsilon_{\mathrm{me}}$ and $\varepsilon_{\mathrm{mg}}$ are the ground state energy and excited state energy of the related electron, respectively, and $\hbar$ is the reduced Planck's constant.

The excited electron energy may be subsequently transferred to the adjacent nanoparticles quickly by the strong SDD interaction between nanoparticles and the related molecules as shown in Figure 13(b). This energy transferring process conforms to energy conservation, so it could be regarded as an electron dipole–dipole resonance (EDDR). The quantum transition rate can be determined by the SDD interaction and could also be described by Fermi golden rule [17].

$$W_{\mathrm{EDDR}} = \frac{2\pi}{\hbar}\sum_{\varphi_{\mathrm{e}},\varphi_{\mathrm{g}}}|\langle\varphi_{\mathrm{e}}|\langle\psi_{\mathrm{g}}|H_{\mathrm{dd}}|\psi_{\mathrm{e}}\rangle|\varphi_{\mathrm{g}}\rangle|^2\delta[\varepsilon_{\mathrm{me}} + \varepsilon_{\mathrm{g}} - \varepsilon_{\mathrm{mg}} - \varepsilon_{\mathrm{e}}], \tag{81}$$

where W_{EDDR} is the quantum transition rate caused by EDDR, and $|\varphi_{\mathrm{g}}\rangle$ and $|\varphi_{\mathrm{e}}\rangle$ are the ground state and excited state wave functions of electron in the nanoparticle, respectively.

This EDDR can display some unique characteristics. First, it is a physical process and cannot associate with charge transfer between the nanoparticle and the adsorbed molecules. So, the EDDR cannot cause alterations for the molecular bonds of the related adsorbed molecules. Second, the EDDR can be suitable for arbitrary electron energy transfer and thereby it might be widespread in various physical systems. Owing to the strong SDD interaction, the quantum transition rate stemming from EDDR may far exceed that for the fluorescence emission. Hence, most of the photon energy absorbed by electrons in the molecules may be fast transferred to the electrons in the neighboring nanoparticles so that the fluorescence emission of the molecules would be suppressed greatly.

According to this EDDR mechanism, the quenching of fluorescence may be dominated by several vital factors. One is the distance between the nanoparticle and the molecules. And a smaller distance usually leads to a stronger SDD interaction and EDDR, which can quench the fluorescence more seriously. Another one is the polarizability of the nanoparticle. Generally speaking, metallic nanoparticles with higher electric conductivity $\sigma(0)$ usually possess a larger electrostatic polarizability, thereby yielding a stronger SDD interaction and EDDR, *i.e.*, $H_{\mathrm{dd}} \propto [\sigma(0)]^4$. Therefore, the existence of metallic nanoparticles such as Ag, Au, and Cu nanoparticles with good electric conductivity would be anticipated to lead to obvious quenching of fluorescence, which may be verified by the experimental results [63,64]. The third one is the relaxation strain and the mechanical-electric coupling strength of the metallic nanoparticle. A larger surface relaxation strain and a larger mechanical-electric coupling strength may induce a stronger SDD interaction and a stronger EDDR which may suppress the fluorescence emission of neighboring molecules more effectively. The fourth one is the temperature. As the temperature decreases, the electric conductivity of metals usually increases gradually, which enhances the SDD interaction and EDDR, resulting in a more severe quenching of fluorescence for the neighboring molecules.

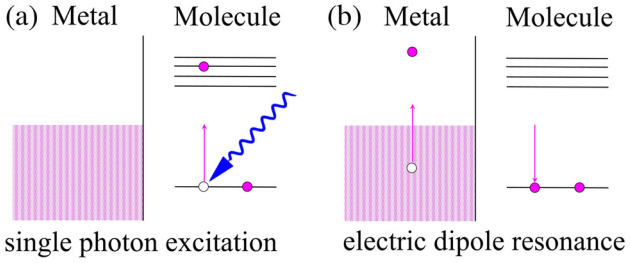

Figure 13: Schematic diagram of a possible mechanism for suppression of fluorescence owing to electric dipole resonance. The magenta circles represent electrons, the blue curved arrow stands for an incident photon and the magenta arrows show the electron hopping between different states (black horizontal lines). (a) single photon absorption process at the molecule; and (b) electron energy transfer by means of electric dipole resonance between the molecule (right) and an adjacent metallic nanoparticle (left).

2.2.11 Surface-enhanced Raman scattering (SERS)

SERS was first observed in 1970s [65–67] and it could be utilized as an ultra-sensitive analytical technique to detect a minor amount of molecules in terms of the fingerprint Raman spectrum. Since its discovery, it has attracted worldwide attention and has brought several tens of thousands of publications in which several recent reviews have given excellent introduction and summaries [68–70]. For the

scientific origin of SERS, many theoretical attempts have been made to understand various experimental phenomena on SERS since the discovery of SERS. By means of worldwide research in recent several decades, it is popularly believed to originate from two mechanisms. One is the electromagnetic enhancement associated with the surface plasma excitations, which is usually regarded as the main mechanism of SERS [68–70]. The other is the chemical enhancement resulting from charge transfers between the metal nanoparticles and adsorbed target molecules [68–70]. Despite that these theoretical models could capture some physics on SERS, no model could clarify all the important phenomena revealed by various SERS experiments. So, for the further development and wide applications of SERS in multifields, constructing a unified theoretical model for SERS may be very necessary, but it is very challenging and is still an open topic [68–70].

Upon SERS, a successful model must answer the important questions below.

1) Why does the Raman band shift in the SERS experiments?
2) What are the reasons for the Raman band fluctuations?
3) Why does the externally applied voltage influence the Raman intensity?
4) Why do the semiconductor nanoparticles generate SERS?
5) Why can the sharp surface features such as sharp edges, corners, and nano-stars yield notable SERS?
6) Why can the SERS yield so large an enhanced factor (EF)?
7) Why can hotspots enhance the EF?
8) What is the physical mechanism for the distance dependence of SERS?
9) Why does the SERS sensitively depend on frequency of incident laser?
10) What are the selection rules for the SERS?

In this section, by employing the discovered strong electrostatic field, the related SDD and the resultant EDDR between the nanoparticles and the neighboring molecules, a new physical mechanism for the SERS is proposed and utilized to understand the vital phenomena on SERS.

By means of the quantum second-order perturbations [17], considering the single quantum excitation in the nanoparticle (the quantum excitation in metal nanoparticles may be the excitation of the localized surface plasmon, but it may be the creation of electron–hole pair in semiconductors) and the EDDR between nanoparticle and adsorbed molecules as shown in Figure 14, the quantum transition coefficient from the ground state to the intermediate virtual state of electron in a molecule is given by

$$C_{\mathrm{i}\leftarrow\mathrm{g}}(\vec{q},\omega)=\frac{eE_0}{im_{\mathrm{e}}\omega}\times\sum_{\varphi_{\mathrm{e}},\varphi_{\mathrm{g}}}\frac{\langle\varphi_{\mathrm{g}}|\langle\psi_{\mathrm{i}}|H_{\mathrm{dd}}|\psi_{\mathrm{g}}\rangle|\varphi_{\mathrm{e}}\rangle\langle\varphi_{\mathrm{e}}|e^{i\vec{q}\cdot\vec{r}}\vec{e}\cdot\vec{p}|\varphi_{\mathrm{g}}\rangle}{(\varepsilon_{\mathrm{mg}}-\varepsilon_{\mathrm{mi}}+\hbar\omega+i\eta)(\varepsilon_{\mathrm{g}}-\varepsilon_{\mathrm{e}}+\hbar\omega+i\eta)}, \tag{82}$$

where $C_{\mathrm{i}}(q,\omega)$ is the wavevector q and angular frequency ω dependence of the quantum transition coefficient, m_{e} is the electron mass, E_0 is the magnitude of electric field of the laser, $\vec{e}$ is the polarization unit vector of the incident laser beam, $\vec{p}$ is the momentum operator, $\hbar$ is the reduced Planck's constant, $|\varphi_{\mathrm{e}}\rangle$ and $|\varphi_{\mathrm{g}}\rangle$ present the ground state wave function and the electronic excited state wave function in the nanoparticles, ε_{e} and ε_{g} are the corresponding eigenenergy for the states, $|\psi_{\mathrm{i}}\rangle$ and $|\psi_{\mathrm{g}}\rangle$ are the intermediate virtual state and the ground state of electron in the molecules, $\varepsilon_{\mathrm{mi}}$ and $\varepsilon_{\mathrm{mg}}$ are the corresponding energy levels for the intermediate state and ground state, respectively.

This quantum transition coefficient may determine the pumping process of SERS and the related EF. And the radiated power of Raman scattering is given by [69,71]

$$P_{\mathrm{Raman}}=\frac{(\omega\pm\omega_{\mathrm{q}})^4}{12\pi\varepsilon_0}|\vec{P}(\omega\pm\omega_{\mathrm{q}})|^2, \tag{83}$$

where ω_{q} is the frequency of molecular vibration mode, ε_0 is the vacuum permittivity, and $P(\omega\pm\omega_{\mathrm{q}})$ is the oscillating electric dipole of the molecules.

Combining the quantum transition coefficient from ground state to the intermediate virtual state and the power of Raman scattering, one may obtain

$$P_{\mathrm{SERS}}\propto\frac{(\omega\pm\omega_{\mathrm{q}})^4\left(n_{\mathrm{q}}+\frac{1}{2}\mp\frac{1}{2}\right)}{12\pi\varepsilon_0}E_0^2\sum_{\gamma\rho}|\alpha_{\gamma\rho}^{\mathrm{SERS}}|^2, \tag{84}$$

$$\alpha_{\mu\nu}^{\mathrm{SERS}}=\sum_{\varphi_{\mathrm{e}},\varphi_{\mathrm{g}}}^{\psi_{\mathrm{i}},\psi_{\mathrm{g}}}\frac{\langle\varphi_{\mathrm{g}}|\langle\psi_{\mathrm{i}}|H_{\mathrm{dd}}|\psi_{\mathrm{g}}\rangle|\varphi_{\mathrm{e}}\rangle\langle\varphi_{\mathrm{e}}|\mu_{\mu}'|\varphi_{\mathrm{g}}\rangle\langle\psi_{\mathrm{g}}|\mu_{\nu}|\psi_{\mathrm{i}}\rangle}{(\varepsilon_{\mathrm{mg}}-\varepsilon_{\mathrm{mi}}+\hbar\omega+i\eta)(\varepsilon_{\mathrm{g}}-\varepsilon_{\mathrm{e}}+\hbar\omega+i\eta)}, \tag{85}$$

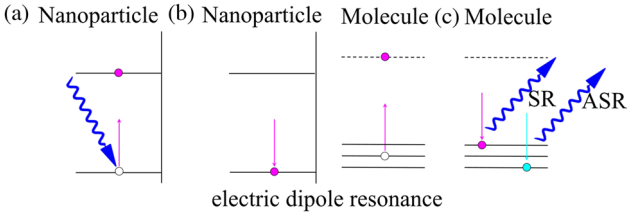

Figure 14: Schematic diagram of quantum processes for SERS. (a) creation of an electron excitation by absorbing a photon (curved blue arrow); (b) the energy transfer in terms of EDDR between nanoparticle and adsorbed molecules; and (c) emission of Stokes Raman emission or emission of anti-Stokes Raman photon.

where n_q is the number of molecular vibrations, $\alpha_{\mu\nu}^{SERS}$ is the component of effective polarizability tensor for SERS, the subscripts μ and ν are the incident photon polarization direction and the scattered photon polarization direction in Cartesian coordinates (x, y, z), μ is the Stokes (anti-Stokes) dipole moment operator for the molecules, and μ' is the dipole moment operator for the nanoparticle. This effective polarization tensor determines the selection rules for SERS.

The single-molecule EF (SMEF) of SERS could be estimated by

$$EF_{sm}(\vec{k},\omega) \approx \left|\frac{l_0^3}{(2\pi)^2 r_i^3}\varepsilon_{n2}(\vec{k},\omega)\right|^2 \left|\frac{\alpha_n(0)E_n}{\alpha_n(\vec{k},\omega)E_0}\frac{\alpha_m(0)E(r_i)}{\alpha_m(\vec{k},\omega)E_0}\right|^2, \quad (86)$$

where $\alpha_n(k,\omega)$ is the momentum vector k and angular frequency ω dependence of polarizability of nanoparticles, $\alpha_m(k,\omega)$ is the momentum vector k and angular frequency ω dependence of polarizability of molecules, $\alpha_n(0)$ and $\alpha_m(0)$ are the electrostatic polarizability of nanoparticles and molecules, respectively, $\varepsilon_{n2}(k,\omega)$ is the imaginary part of relative dielectric constant of the nanoparticles, E_n is the electrostatic field in the nanoparticle due to the surface strain relaxation, and $E(r_i)$ is the position r_i dependence of the electrostatic field experienced by the molecule.

Eq. (86) shows that the SMEF strongly depends on the distance between the nanoparticle and the molecules. Based on the distance dependent SDD magnitude shown in Eqs. (56) and (79), the overall $EF(k,\omega)$ may be $EF_{sm}(k,\omega)4\pi(R_0 + r)^2$, thus

$$\begin{aligned} EF(\vec{k},\omega) &\propto \frac{(R_0+r)^2}{r^{10}} \quad (r < l_0);\\ EF(\vec{k},\omega) &\propto \frac{(R_0+r)^2}{r^{12}} \quad (l_0 < r < 2R_0);\\ EF(\vec{k},\omega) &\propto \frac{(R_0+r)^2}{r^{14}} \quad (2R_0 < r); \end{aligned} \quad (87)$$

Since the radius R_0 of the utilized nanoparticle is usually much larger than the surface relaxation length l_0, *i.e.*, $R_0 \gg l_0$, the overall $EF(k,\omega)$ may decay with r^{-10} in the near-field range $r < l_0$, which was verified by experimental observations [72].

As indicated by Eq. (86), the EF of SERS may obviously depend on the frequency (wavelength) of the incident light. The imaginary part of relative dielectric function of a system is proportional to its absorption coefficient [17,43], so the EF of SERS may reach its peak value when the frequency (wavelength) of light is coincident with the characteristic frequency (wavelength) of the maximum absorption coefficient of the nanoparticle, which is the commonly observed experimental results [73,74].

Also shown by this equation is that not only the metal nanoparticles but also the semiconductor nanoparticles that possess a large static polarizability $\alpha_n(0)$ and a large imaginary part of dynamic polarizability $\varepsilon_{2n}(\omega)$ may give birth to a noticeable SERS, which was verified by experimental observations [75,76].

Based on Eq. (86), one may understand the vital role of the sharp surface features in the SERS. The sharp surface features such as nano-star, sharp edges, and shared corners mean that there exist many regions with dramatic strain relaxation. The strain relaxation in these regions may further generate a strong electrostatic field and an apparent net charge accumulation according to Eqs. (1) and (53). The net charges at sharp edges and shared corners will yield an intensely electrostatic field and thereby cause a strong SDD interaction between neighboring molecules and the surface regions with sharp features, as may lead to a notable SERS. So the regions close to the sharp edges and corners may behave as the active spots for SERS and the size of these active spots may be the order of the surface relaxation length l_0, *i.e*, several atomic layers ~1 nm [53,57,59]. For the nanoparticle agglomeration systems, the electrostatic field in the nano-gap between two nanoparticles may be greatly enhanced due to more mutually induced charges at the confronting side of the other nanoparticle. Therefore, the SDD and EDDR between nanoparticles and molecules in the nano-gap may be conspicuously enhanced, resulting in a more notable SERS. The regions in the nano-gap may be the hotspots which have already been revealed in many experiments [70,77]. Based on the nanometer sized surface relaxation length l_0, the hotspot size may be the order of ~1 nm, which is in accord with the experimental results [70,77,78].

As stated in the Section 2.2.9, the intense electrostatic field generated by surface sharp features such as sharp edges and corners would bring alterations for the covalent bond strength of the molecules, thereby resulting in the Raman band shift for the nearby molecules especially those adsorbed at positions with the surface sharp features. In terms of a simple estimation, the largest shift of Raman band may reach several percent. And as a rule, a bigger Raman shift usually corresponds to a larger SMEF of SERS. It is because a bigger Raman shift may usually be correlated with a more intensive electrostatic field which may further induce a stronger EDDR and a larger EF. In the SERS experiments, due to the randomness and disorder of the sharp features at nanoparticle surfaces, the yielded electrostatic field may also exhibit complexity which may subsequently induce a distinct Raman shift, Raman intensity, spectral shape, and EF of SERS in different experiments even with the same type of nanoparticles as the SERS substrate. This

may be confirmed by the commonly encountered experimental observations on the SERS fluctuations such as intensity fluctuation, spectral shape fluctuation, Raman peak position fluctuation, and Raman peak width fluctuation [79].

In the previous experimental investigations, the experimental observations that SERS intensity relied on the electrochemical potential of substrate was recognized as a strong evidence for the chemical enhancement mechanism dominated by charge transfer between the SERS substrate and the adsorbed molecules [70]. However, a quite different and complete physical mechanism for the effect of electrochemical potential on SERS may be put forward here. An externally applied electric voltage on the SERS substrate would change the electrostatic field exerted on the adsorbed molecules. Therefore, both the SDD interaction and EDDR may be greatly altered, which may further result in the obvious variations in the SERS intensity. A simple comparison between this mechanism and chemical enhancement could be performed. Chemical enhancement requires charge transfer, but the EDDR mechanism may require charge separation induced by the strains at the sharp surface features. The chemical enhancement occurs only for the chemically adsorbed molecules, but the EDDR mechanism may be valid for the physically adsorbed molecules several nanometers away. The discovery of the so-called shell-isolated nanoparticle-enhanced Raman spectroscopy where the metal nanoparticles were coated by ultrathin semiconductor films [70,80,81] preventing direct interaction between nanoparticles and adsorbates may disagree with the chemical enhancement mechanism, but might be consistent with EDDR mechanism.

The selection rules of SERS may be altered by the EDDR between SERS substrate and the adsorbed molecules, as is indicated by Eqs. (78) and (85). In the equations, the amplitude of the diagonal terms $\langle\varphi_g|P_{e\gamma}|\varphi_e\rangle\langle\varphi_e|\mu'_\mu|\varphi_g\rangle$ ($\mu = \gamma$), $\langle\psi_i|p_{i\rho}(\vec{r_i})|\psi_g\rangle\langle\psi_g|\mu_\upsilon|\varphi_i\rangle$ ($\nu = \rho$) may be much larger than other off-diagonal terms $\langle\varphi_g|P_{e\gamma}|\varphi_e\rangle\langle\varphi_e|\mu'_\mu|\varphi_g\rangle(\mu\neq\gamma)$, $\langle\psi_i|p_{i\rho}(\vec{r_i})|\psi_g\rangle\langle\psi_g|\mu_\upsilon|\varphi_i\rangle$ ($\nu \neq \rho$), thus these approximations may be appropriate,

$$\begin{aligned}&\langle\varphi_g|P_{e\gamma}|\varphi_e\rangle\langle\varphi_e|\mu'_\mu|\varphi_g\rangle \propto \delta_{\mu\gamma}\\&\langle\psi_i|p_{i\rho}(\vec{r_i})|\psi_g\rangle\langle\psi_g|\mu_\nu|\psi_i\rangle \propto \delta_{\nu\rho}.\end{aligned} \tag{88}$$

where the Kronecker symbol is $\delta_{\mu\gamma} = 1$ for the case $\mu = \gamma$, otherwise it is zero. These approximations may be applicable for the nanoparticles and molecules without off-diagonal terms in their respective polarizability tensors. So, the effective polarizability tensor for SERS may be given by

$$\begin{aligned}\alpha_{\mu\nu}^{\mathrm{SERS}} &= \sum_{\varphi_e,\varphi_g}^{\psi_i,\psi_g} \frac{\langle\varphi_g|P_{e\mu}|\varphi_e\rangle\langle\varphi_e|\mu'_\mu|\varphi_g\rangle\langle\psi_g|\mu_\nu|\psi_i\rangle\langle\psi_i|p_{i\nu}(\vec{r_i})|\psi_g\rangle}{(\varepsilon_{mg} - \varepsilon_{mi} + \hbar\omega + i\eta)(\varepsilon_g - \varepsilon_e + \hbar\omega + i\eta)} \\ &\times \frac{1}{4\pi\varepsilon_0}\sum_i\left(\frac{\delta_{\mu\nu}}{|\vec{r_i}|^3} - \frac{3r_{i\mu}r_{i\nu}}{|\vec{r_i}|^5}\right).\end{aligned} \tag{89}$$

This equation could point out that the effective polarizability tensor for SERS may determine the selection rules of SERS. Some normal Raman-active vibration mode may be silent when the molecules at the positions fulfill the conditions $3r_{i\mu}r_{i\mu} = (r_i)^2$. Furthermore, it may reveal that the TEF at the metal nanoparticle surfaces can give rise to some additional contributions to the Raman scattering, *i.e.*, the off-diagonal term in the round brackets in Eq. (89). And the off-diagonal term could activate the forbidden vibration mode in the common Raman scattering. It may be the physical origin of popular experimental observations of the forbidden Raman mode in SERS [82–84].

To examine whether this EDDR mechanism grasps the physics of SERS or not, the magnitude of SMEF should be estimated. The electrostatic field within the strain relaxation length of nanoparticle may reach a magnitude ~10^8 V/m, and the field $E(r_i)$ applied on the adsorbed molecules at the edges and corners may be in the range 10^8–10^9 V/m. The electric field E_0 of the incident laser in the experiments was usually ~10^6 V/m which corresponds to a laser radiation power density ~10^5 W/cm^2 [82,83]. In the cases that the metal nanoparticles were used as the SERS substrate, the SMEF could be obtained by using the relative dielectric function of metals [17,43].

$$\mathrm{EF}_{\mathrm{sm}}(\vec{k},\omega) \approx \left|\frac{l_0^3}{(2\pi)^2 r_i^3}\frac{\sigma(0)}{\varepsilon_0\omega}\right|^2\left|\frac{E_n}{E_0}\frac{\alpha_m(0)E(r_i)}{\alpha_m(\vec{k},\omega)E_0}\right|^2, \tag{90}$$

where $\sigma(0)$ is the direct current electrical conductivity of the metal, and ε_0 is the vacuum permittivity. If the electrostatic polarizability of molecules is comparable to its dynamic polarizability, the optimum SMEF could be estimated to reach a value as high as 10^8–10^{10} in the experiments using metal nanoparticles Ag, Au, and Cu as SERS substrate. The estimated optimum SMEF was found to agree with the conclusions [69,70] obtained from many experimental observations.

Meanwhile, the yielded electric field on the molecules $E(r_i)$ may be proportional to the amount of separated charges in the metal nanoparticle. The amount of separated charges is usually proportional to the static polarizability, so

the field $E(r_i)$ may be proportional to the static polarizability of metal nanoparticle, *i.e.*, $E(r_i) \propto \alpha_n(0)$. Furthermore, according to the static conductivity and the relative dielectric function of metals [17,43], a relation $\alpha_n(0) \approx [\sigma(0)]^2/\varepsilon_0\omega_p{}^2$ may exist. Therefore, the SMEF employing the metal nanoparticles as the SERS substrate may follow the relation $EF_{sm}(k, \omega) \propto [\sigma(0)]^6/(\varepsilon_0\omega_p{}^2)^2$. On the other hand, the electric field in the strain relaxation length l_0 remarkably relies on the mechanical-electric coupling strength and the surface strain of the nanoparticles. Combining these factors, the following relation may be valid for SMEF using a metal substrate:

$$EF_{sm}(\vec{k}, \omega) \propto \frac{[\sigma(0)]^6}{(\varepsilon_0\omega_p^2)^2}\left|\frac{\partial E_F}{e\partial\xi_{ij}}\xi_{ij}\right|^4. \tag{91}$$

As shown, the SMEF depends on the electric conductivity $\sigma(0)$, the mechanical-electric coupling strength $|\partial E_F/\partial\xi_{ij}|$, and the surface strains ξ_{ij}. Hence, the metal nanoparticles such as Ag, Au, and Cu exhibiting much higher electrical conductivity than other transition metals can usually result in much stronger SERS, which was the experimental observations [85–88].

As indicated by the above analysis, the proposed simple mechanism based on EDDR between the SERS substrate and the neighboring molecules may grasp the physics of SERS and could help people understand the complex phenomena on SERS deeply.

The important role of EDDR has been discussed for the suppression of fluorescence and SERS in this work. The EDDR is a highly efficient energy transfer channel between nanoparticles and their nearby systems such as nanoparticles and molecules. To be anticipated, it can also play an important role in other fields such as tip-enhanced Raman scattering and nanoparticle-assisted photocatalysis.

2.2.12 MEMS

The MEMS finds wide applications in many areas, for instance, the MEMS are employed as micro-sensors and micro-actuators. It has been experimentally established that the pull-in instability usually happens and thereby the MEMS collapses when the applied electrostatic voltage reaches the pull-in voltage [89–91]. To manufacture and control the MEMS well in the industry, the important issue is the thorough understanding of the MEMS at the microscale. Therefore, the physical model of MEMS is required and has attracted much attention over the past several decades. Besides the conventional electrostatic forces, other physical factors such as effective stiffness, dielectric charging effect, stress gradient effect, and temperature effect were considered and the models were built [89,90,92]. However, another important electrostatic force originating from the mechanical-electric coupling has been neglected over the past years. It may play an import role for the performances of MEMS devices and would be uncovered in the following discussions.

To reveal the new electrostatic force, a simple spring–mass system is taken as an example. But the discovered new electrostatic force and the method used in the following discussions may also apply for other configurations of the MEMS not restricted to the simple spring–mass system.

For a simple lumped spring–mass system under an externally applied potential U_e, the precise electrostatic potential outside the metal plates could be expressed by Eq. (5),

$$\varphi(\vec{r}) = \varphi_i(\vec{r}) + \varphi_e(\vec{r}),$$

where $\varphi_i(r)$ is the intrinsic potential due to the non-uniform Fermi levels in the metal plates, $\varphi_e(r)$ is the external electrostatic potential including the contribution from the induction charges at the metal surfaces. They satisfy the constraint conditions in the concerned volume V outside the metal plates.

$$\nabla^2\varphi_i(\vec{r}) = 0$$
$$\nabla^2\varphi_e(\vec{r}) = 0$$

It means that there is no charge outside the metal plates. The boundary conditions of the intrinsic potential $\varphi_i(r)$ is given by

$$\varphi_{i1}(\vec{r}) = \varphi_i(\vec{r})|_{S1}$$
$$\varphi_{i0}(\vec{r}) = \varphi_i(\vec{r})|_{S0}$$

And the boundary conditions of the potential $\varphi_e(r)$ is

$$\varphi_e(\vec{r})|_{S1} = U_e$$
$$\varphi_e(\vec{r})|_{S0} = 0$$

where $S0$ stands for the surface of the unmovable metal plate during the MEMS device operation, and $S1$ is the surface of the movable metal plate, as is schematically shown in Figure 15. The total electrostatic energy in the concerned volume V is given by

$$W = \frac{1}{2}\varepsilon_0\varepsilon\int_V[\nabla\varphi_i(\vec{r})]^2 dV + \frac{1}{2}\varepsilon_0\varepsilon\int_V[\nabla\varphi_e(\vec{r})]^2 dV + \varepsilon_0\varepsilon\int_V\nabla\varphi_i(\vec{r})\cdot\nabla\varphi_e(\vec{r})dV. \tag{92}$$

where ε is the dielectric constant of medium between two metal plates. Using the constraint conditions the total

electrostatic energy could be simplified to be

$$W = -\frac{1}{2}\varepsilon_0\varepsilon \int\limits_{S1+S0} \varphi_{\mathrm{i}}(\vec{r})\nabla\varphi_{\mathrm{i}}(\vec{r})\cdot \mathrm{d}s - \frac{1}{2}\varepsilon_0\varepsilon \int\limits_{S1+S0} \varphi_{\mathrm{e}}(\vec{r})\nabla\varphi_{\mathrm{e}}(\vec{r})\cdot \mathrm{d}s - \varepsilon_0\varepsilon \int\limits_{S1+S0} \varphi_{\mathrm{e}}(\vec{r})\nabla\varphi_{\mathrm{i}}(\vec{r})\cdot \mathrm{d}s.$$

It can be further simplified using the assumption of the intrinsically neutral metals and the boundary conditions for both the intrinsic potential $\varphi_{\mathrm{i}}(r)$ and the external electrostatic potential $\varphi_{\mathrm{e}}(r)$ as follows:

$$W = -\frac{1}{2}\varepsilon_0\varepsilon\int_{S1}\varphi_{\mathrm{i}1}(\vec{r})\nabla\varphi_{\mathrm{i}1}(\vec{r})\cdot \mathrm{d}s - \frac{1}{2}\varepsilon_0\varepsilon\int_{S0}\varphi_{\mathrm{i}0}(\vec{r})\nabla\varphi_{\mathrm{i}0}(\vec{r})\cdot \mathrm{d}s + \frac{1}{2}CU_{\mathrm{e}}^2. \tag{93}$$

During the operation of the MEMS devices, the movable metal plates are usually subject to non-uniform deformation which was addressed earlier [93]. So, the related intrinsic potential could be divided into two parts. One is the initially intrinsic potential $\varphi_{\mathrm{ii}}(r)$, and the other is the intrinsic potential $\varphi_{\mathrm{iw}}(r)$ induced by the deformation of the MEMS device at work, as shown below.

$$\varphi_{\mathrm{i}1}(\vec{r}) = \varphi_{\mathrm{ii}}(\vec{r}) + \varphi_{\mathrm{iw}}(\vec{r}),$$

$$W = -\frac{1}{2}\varepsilon_0\varepsilon\int_{S1}\varphi_{\mathrm{ii}}(\vec{r})\nabla\varphi_{\mathrm{ii}}(\vec{r})\cdot \mathrm{d}s - \frac{1}{2}\varepsilon_0\varepsilon\int_{S1}\varphi_{\mathrm{iw}}(\vec{r})\nabla\varphi_{\mathrm{ii}}(\vec{r})\cdot \mathrm{d}s - \frac{1}{2}\varepsilon_0\varepsilon\int_{S1}\varphi_{\mathrm{ii}}(\vec{r})\nabla\varphi_{\mathrm{iw}}(\vec{r})\cdot \mathrm{d}s - \frac{1}{2}\varepsilon_0\varepsilon\int_{S1}\varphi_{\mathrm{iw}}(\vec{r})\nabla\varphi_{\mathrm{iw}}(\vec{r})\cdot \mathrm{d}s - \frac{1}{2}\varepsilon_0\varepsilon\int_{S0}\varphi_{\mathrm{i}0}(\vec{r})\nabla\varphi_{\mathrm{i}0}(\vec{r})\cdot \mathrm{d}s + \frac{1}{2}CU_{\mathrm{e}}^2.$$

The initially intrinsic potential $\varphi_{\mathrm{ii}}(r)$ of the metal plate may exhibit random properties so that the following approximations may hold right.

$$-\frac{1}{2}\varepsilon_0\varepsilon\int_{S1}\varphi_{\mathrm{iw}}(\vec{r})\nabla\varphi_{\mathrm{ii}}(\vec{r})\cdot \mathrm{d}s \approx 0$$

$$-\frac{1}{2}\varepsilon_0\varepsilon\int_{S1}\varphi_{\mathrm{ii}}(\vec{r})\nabla\varphi_{\mathrm{iw}}(\vec{r})\cdot \mathrm{d}s \approx 0$$

At last, the totally electrostatic energy may be expressed as follows:

$$W = -\tfrac{1}{2}\varepsilon_0\varepsilon\left[\int_{S1}\varphi_{\mathrm{ii}}(\vec{r})\nabla\varphi_{\mathrm{ii}}(\vec{r})\cdot \mathrm{d}s + \int_{S1}\varphi_{\mathrm{iw}}(\vec{r})\nabla\varphi_{\mathrm{iw}}(\vec{r})\cdot \mathrm{d}s + \int_{S0}\varphi_{\mathrm{i}0}(\vec{r})\nabla\varphi_{\mathrm{i}0}(\vec{r})\cdot \mathrm{d}s\right] + \tfrac{1}{2}CU_{\mathrm{e}}^2.$$

The corresponding electrostatic force between the two metal plates is given by

$$F_{\mathrm{e}} = -\frac{1}{2}\varepsilon_0\varepsilon S\frac{U_{\mathrm{e}}^2}{d^2} + \frac{1}{2}\varepsilon_0\varepsilon\int_{S1}\frac{\partial\varphi_{\mathrm{iw}}E_{\mathrm{iw}}}{\partial d}\mathrm{d}s, \tag{94}$$

where F_{e} is the total electrostatic force between the two metal plates, S is the area of the metal plate, d is the distance of the gap between the metal plates, and E_{iw} is the normal component of electrostatic field arising from intrinsic potential $\varphi_{\mathrm{iw}}(r)$. The utilized metal plate is usually so thin that the edge surfaces could be ignored, and the second term in the above equation can be approximated to be,

$$\frac{1}{2}\varepsilon_0\varepsilon\int_{S1}\frac{\partial\varphi_{\mathrm{iw}}E_{\mathrm{iw}}}{\partial d}\mathrm{d}s \approx \frac{1}{2}\varepsilon_0\varepsilon\left[\int_{S1^+}\frac{\partial\varphi_{\mathrm{iw}}^+E_{\mathrm{iw}}^+}{\partial d}\mathrm{d}s + \int_{S1^-}\frac{\partial\varphi_{\mathrm{iw}}^-E_{\mathrm{iw}}^-}{\partial d}\mathrm{d}s\right],$$

where the potentials φ_{iw}^+ and φ_{iw}^- are the potential $\varphi_{\mathrm{iw}}(r)$ at the surfaces $S1^+$ and $S1^-$, E_{iw}^+ and E_{iw}^- are the corresponding normal electrostatic fields at the surface $S1^+$ and $S1^-$, respectively. The magnitude of the normal electrostatic field E_{iw}^+ is almost the same as the field E_{iw}^-. Since the metal plate is so thin that the strain gradient of the metal plate at work could be regarded as constant and thereby the accumulated net charges at the surface $S1^+$ is opposite to that at the surface $S1^-$ according to Gauss's law. Therefore, the above equation could be written as follows:

$$\frac{1}{2}\varepsilon_0\varepsilon\int_{S1}\frac{\partial\varphi_{\mathrm{iw}}E_{\mathrm{iw}}}{\partial d}\mathrm{d}s \approx \frac{1}{2}\varepsilon_0\varepsilon\int_{S1^+}\frac{\partial(\varphi_{\mathrm{iw}}^+ - \varphi_{\mathrm{iw}}^-)E_{\mathrm{iw}}^+}{\partial d}\mathrm{d}s.$$

Based on Eq. (4), the intrinsic potential difference at the surfaces $S1^+$ and $S1^-$ of the metal plate at work may be given by

$$\varphi_{\mathrm{iw}}^+ - \varphi_{\mathrm{iw}}^- = -\frac{(E_{\mathrm{F}}^+ - E_{\mathrm{F}}^-)}{e},$$

where E_{F}^+ and E_{F}^- are the Fermi levels of the metal at surface $S1^+$ and $S1^-$, respectively. Hence, the total electrostatic forces between the metal plates may be obtained as follows:

$$F_{\mathrm{e}} = F_{\mathrm{e}1} + F_{\mathrm{e}2},$$

$$F_{\mathrm{e}1} = -\frac{1}{2}\varepsilon_0\varepsilon S\frac{U_{\mathrm{e}}^2}{d^2},$$

$$F_{\mathrm{e}2} = -\frac{1}{2}\frac{\varepsilon_0\varepsilon S}{e}\frac{\partial(E_{\mathrm{F}}^+ - E_{\mathrm{F}}^-)E_{\mathrm{iw}}^+}{\partial d}.$$

The first term $F_{\mathrm{e}1}$ is the traditional electrostatic force, and the second term $F_{\mathrm{e}2}$ is the newly uncovered electrostatic force due to the mechanical-electric coupling of metals in the work. The partial differential of the function with respect to the gap d in the second term is always negative, so the newly uncovered electrostatic force is also an attractive electrostatic force.

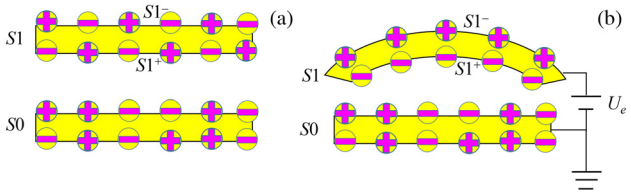

Figure 15: A typical model for the metallic MEMS consisting of two metal plates. (a) the pristine state of MEMS and the initially intrinsic charge distribution; (b) the operation state of the MEMS under the external potential U_e and the generated intrinsic charge distribution due to the deformations of the metal plate.

In terms of rough calculation, the normal electrostatic field E_{iw}^{+} may be approximated as follows:

$$E_{iw}^{+} \approx \frac{\sigma_{iw}}{4\pi\varepsilon_0\varepsilon}\left\{\int_{S1^+}\frac{z_0 dx dy}{(x^2+y^2+z_0^2)^{3/2}} - \int_{S1^+}\frac{(z_0+h)dxdy}{[x^2+y^2+(z_0+h)^2]^{3/2}}\right\},$$

where σ_{iw} is the intrinsic surface charge density of the metal plate at work, h is the thickness of the metal plate, and z_0 is the distance away from the metal surface $S1^+$. The normal electrostatic field E_{iw}^{+} can be obtained by calculating the above simple integrals as follows:

$$E_{iw}^{+} \approx \frac{\sigma_{iw}}{\varepsilon_0\varepsilon}\frac{h}{L},$$

where L is the size of the metal surface and it satisfies the relation $L^2 \approx S$. Using Gauss's law, it satisfies

$$-\varepsilon_0\varepsilon_m\frac{\nabla E_F}{e}S + \varepsilon_0\varepsilon E_{iw}^{+}S \approx \sigma_{iw}S, \tag{95}$$

where ε_m is the static dielectric constant of the metal. So, the normal electrostatic field E_{iw}^{+} is given by

$$E_{iw}^{+} \approx -\frac{\varepsilon_m}{\varepsilon}\frac{\nabla E_F}{e}\frac{h}{L}. \tag{96}$$

Despite the small value of the ratio h/L that is of the order of 10^{-2}, the normal electrostatic field E_{iw}^{+} may be still intensive because the static dielectric constant of the metals is very huge and the ratio $\varepsilon_m/\varepsilon$ is very large. The field could be expressed in another form by taking advantage of the linear strain assumption as follows:

$$E_{iw}^{+} \approx -\frac{\varepsilon_m}{e\varepsilon}\frac{(E_F^{+}-E_F^{-})}{L}$$

Substituting the approximated expression of the field E_{iw}^{+} in the form of newly uncovered electrostatic force yields the following:

$$F_{e2} \approx \frac{1}{2}\frac{\varepsilon_0\varepsilon_m S}{e^2 L}\frac{\partial(E_F^{+}-E_F^{-})^2}{\partial d}.$$

The Fermi level difference can be written as

$$E_F^{+}-E_F^{-} \approx \frac{\partial E_F}{\partial\xi_{ij}}(\xi_{ij}^{+}-\xi_{ij}^{-}),$$

where ξ_{ij}^{+} and ξ_{ij}^{-} denote the strain component at the surface $S1^+$ and $S1^-$, respectively, and $\partial E_F/\partial\xi_{ij}$ is the strain ξ_{ij} dependent mechanical-electric coupling. The subscripts i, j conform to the Einstein summation convention. Many metal crystals exhibit the cubic symmetry, so the Fermi level difference may be simplified further as follows:

$$E_F^{+}-E_F^{-} \approx \frac{\partial E_F}{\partial\xi_V}(\xi_V^{+}-\xi_V^{-})$$

where ξ_V is the volume strain, ξ_V^{+} and ξ_V^{-} are the volume strain at the surface $S1^+$ and $S1^-$, respectively. As a result, the electrostatic force F_{e2} is

$$F_{e2} = \frac{1}{2}\frac{\varepsilon_0\varepsilon_m S}{L}\left(\frac{\partial E_F}{e\partial\xi_V}\right)^2\frac{\partial(\xi_V^{+}-\xi_V^{-})^2}{\partial d}. \tag{97}$$

The volume strain difference for a thin plate may depend on the magnitude of the electrostatic force F_{e1}.

$$(\xi_V^{+}-\xi_V^{-}) = J\frac{F_{e1}}{S},$$

where the coefficient J has the same unit as the elastic compliance, and it depends on the modulus, geometry, and the stress distribution of the metal plate. In general, a more uniform stress distribution will yield a smaller coefficient J. Thus, the electrostatic force F_{e2} is as follows:

$$F_{e2} = -\frac{1}{2}\frac{\varepsilon_0\varepsilon_m(\varepsilon_0\varepsilon)^2 S}{L}\left(\frac{J}{e}\frac{\partial E_F}{\partial\xi_V}\right)^2\frac{U_e^4}{d^5}. \tag{98}$$

Its magnitude depends on the mechanical-electric coupling strength $|\partial E_F/\partial\xi_V|$, the magnitude of the coefficient J, the externally applied potential U_e, and the distance of the gap d. Upon the operation of a specific MEMS device, the attractive electrostatic force F_{e2} increases much more rapidly than the traditional electrostatic force F_{e1} as the gap d decreases. The attractive electrostatic force F_{e2} can reduce the pull-in voltage and is harmful for the design and operation of the MEMS devices. So, its magnitude needs to be estimated. The force F_{e2} can be given in another form as follows:

$$F_{e2} = -\frac{2\varepsilon_0\varepsilon_m S}{L}\left(\frac{\partial E_F}{e\partial\xi_V}\right)^2\frac{(\xi_V^{+}-\xi_V^{-})^2}{d}. \tag{99}$$

When the external voltage U_e approaches the pull-in voltage, the ratio between the force F_{e2} and F_{e1} is as follows:

$$\frac{F_{e2}}{F_{e1}} = \frac{4\varepsilon_m}{\varepsilon dL}\left(\frac{\partial E_F}{e\partial\xi_V}\right)^2\frac{(\xi_V^+ - \xi_V^-)^2}{E_e^2}, \quad (100)$$

where E_e is the electrostatic field induced by the external potential U_e between the two- parallel metal plates and its magnitude is $E_e = U_e/d$ presenting the order of 10^6 V/m according to the operational state of the MEMS devices [90]. The volume strain difference of the MEMS structure is experimentally found to be the order of 0.1% [94,95]. The mechanical-electric coupling strength $|\partial E_F/\partial\xi_V|$ could take the estimated value 10 eV. The gap d between the metal plates and the length of the plate is popularly designed to be the order of 3 μm and 10^2 μm [90], respectively. The ratio is thereby estimated to be $F_{e2}/F_{e1} \sim 10^{-6}\varepsilon_m/\varepsilon$. The metals may exhibit very huge static dielectric constant. Therefore, the newly uncovered force F_{e2} should be taken into account for the design and fabrication of MEMS devices. In another respect, the electrostatic field E_{iw}^+ originating from the deformation of the metal plate at work may reach $E_{iw}^+ \sim 10^2\varepsilon_m/\varepsilon$ V/m according to Eq. (100). It may surpass the breakdown strength of a gas which is about 3×10^6 V/m at room temperature and atmospheric pressure [96]. Overall, when the metal plate of the MEMS device is deformed, both the newly revealed attractive electrostatic force F_{e2} and the electrostatic field E_{iw}^+ may be the important factors that enable the MEMS device to collapse. To improve the performance of the metallic MEMS device, the selection of metal with small mechanical-electric coupling strength $|\partial E_F/\partial\xi_V|$ may be a rational route. Another possible route may resort to the designs that make the strain in the metal plate more uniform and avoid the apparent strain gradient.

In the subsection for MEMS the newly attractive electrostatic force F_{e2} and the related electrostatic field E_{iw}^+ are revealed based on the mechanical-electric coupling of the metals and Yuheng Zhang equation. Their physical effects on the operation of various MEMS devices should be quantitatively analyzed in the future.

Furthermore, other important fields such as the fractal antenna for multi-band telecommunication [97–102] and the physical mathematical modeling with fraction order [103,104] have made notable progresses in the recent years. The roles of TEF and the mechanical-electric coupling in these rapidly developing fields should be investigated carefully in the future.

3 Conclusion

In summary, contrary to the long-term classical belief in electrodynamics that the TEF is zero at the metal surface, the TEF at the metal surfaces may be discovered in the work. The TEF at the metal surface and the related electrostatic field inside the metal may give birth to more accurate descriptions of the classical electrostatics of metals, *e.g.*, EEC, EBC, uniqueness theorem, method of image charges, electrostatic shielding, Thompson's theorem, and Green's reciprocation theorem. Interestingly, an intrinsically intensive electrostatic field was found to accompany the nanoparticles, which may lead to the EDDR between the nanoparticle and the nearby molecules. To be excited, a simply unified theoretical model for SERS which is a longstanding problem in physics and chemistry may be constructed by using EDDR in the work. This model may capture the main physics of SERS through the analysis of experimental phenomena on SERS. Besides, when the MEMS operates and a metal plate is deformed, a newly electrostatic field and a newly attractive electrostatic force between two parallel metal plates may be uncovered in terms of the mechanical-electric coupling of the metals. They may be the key factors for the design and fabrication of high-performance MEMS devices in industry. In light of the importance of the mechanical-electric coupling as discussed in the work, a future development of the ongoing research is to obtain the quantitative mechanical-electric coupling strength. Overall, the discovered TEF at the metal surface and the related electrostatic field inside the metal may update people's understanding of the electrostatics of metals and find vital applications in various areas such as SERS and MEMS.

Acknowledgments: The author is grateful for the encouragement from the kind colleagues Liusen Hu, Mu Li, Qifeng Chen, Guangfu Ji, and Hua Li.

Funding information: The author states no funding involved.

Author contributions: The author has accepted responsibility for the entire content of this manuscript and approved its submission.

Conflict of interest: The author states no conflict of interest.

References

[1] Feynman R, Leighton RB, Sands ML. The Feynman Lectures on Physics. Vol. 2. Boston, USA: Pearson Education, Inc., Publishing as Prentice Hall, Inc; 2004. p. 1–10.

[2] Pollack GL, Stump DR. Electromagnetism. 1st edn. Boston, USA: Pearson Education, Inc., Publishing as Addison Wesley; 2002. p. 94.

[3] Cheng DK. Field and Wave Electromagnetics. 2nd edn. Boston, USA: Pearson Education, Inc., Publishing as Addison Wesley; 1989. p. 101–2.

[4] Guo SH. Electrodynamics. 3rd edn. Beijing: Higher Education Press; 2008. p. 37, 40, 43–47, 53–56.
[5] Rose BA. Measurements on contact potential difference between different faces of copper single crystals. Phys Rev. 1933;44:585.
[6] Rivière JC. Contact potential difference measurements by the Kelvin method. Proc Phys Soc B. 1957;70(7):676.
[7] Robertson NA, Blackwood JR, Buchman S, Byer RL, Camp J, Gill D, et al. Kelvin probe measurements: investigations of the patch effect with applications to ST-7 and LISA. Cl Quantum Grav. 2006;23:2665–80. doi: 10.1088/0264-9381/23/7/026.
[8] Yin H, Bai YZ, Hu M, Liu L, Luo J, Tan DY, et al. Measurements of temporal and spatial variation of surface potential using a torsion pendulum and a scanning conducting probe. Phys Rev D. 2014;90(122001):1–5.
[9] Huang YJ. Yuheng Zhang effect: strain-induced electric effect in metals. J Mater Sci Appl. 2019;5(3):58–62.
[10] Huang YJ. Strain induced electric effect in condensed matters. J Mater Sci Appl. 2019;5(3):44–57.
[11] Huang YJ. Electric features of dislocations and electric force between dislocations. Math Mech Solid. 2021;26(4):616–28.
[12] Gibbs JW. On the equilibrium of heterogeneous substances. Trans Conn Acad Arts Sci. 1874–78;3:108–248, 343–524. doi: 10.2475/ajs.s3-16.96.441.
[13] Freedman JF. Residual stress in single-crystal nickel films. IBM J Res Dev. 1962;6(4):449–55.
[14] Ame´lie M, Mathieu F, Manuel F, Nicolas G, Serge K, Pascale K, et al. Residual stress determination in a shot-peened nickel-based single-crystal superalloy using X-ray diffraction. J Appl Cryst. 2015;48:1761–76.
[15] Bechstedt F. Principles of Surface Physics. Berlin: Springer-Verlag Berlin Heidelberg; 2003. p. 293–315.
[16] Feng D, Jin GJ. Condensed Matter Physics (Volume I). Beijing: Higher Education Press; 2013. p. 218–9.
[17] Grosso G, Parravicini GP. Solid state physics. 1st edn. Singapore: Elsevier(Singapore) Pte Ltd; 2006. p. 397, 417, 427–9, 434, 469–71.
[18] Cai SS, Zhu Y, Xu JJ. Electrodynamics. 2nd edn. Beijing: Higher Education Press; 2002. p. 2, 63, 86–91.
[19] Griffiths DJ. Introduction to electrodynamics. 4th edn. Cambridge University Press; 2013. p. 82, 98, 100–1, 119–30.
[20] Rothwell EJ, Cloud MJ. Electromagnetics. 3rd edn. Boca Raton, FL: CRC press, Taylor & Francis Group, LLC; 2018. p. 77–81, 165–7, 233–4.
[21] Zangwill A. Modern electrodynamics. UKCambridge University Press; 2012. p. 133–4, 199–200.
[22] Landau LD, Lifshitz EM. Electrodynamics of continuum media. Beijing: People's Education Press; 1963. p. 13–8. Zhou Qi (translation).
[23] Jackson JD. Classical electrodynamics. 3rd edn. USA: John Wiley & Sons; 1998. p. 57–64.
[24] Maxwell JC. A Treatise on Electricity and Magnetism. 3rd edn. Oxford, 1904, Ge Ge (translated). Wuhan: Wuhan Press; 1994. p. 89–91.
[25] Plimpton SJ, Lawton WE. A very accurate test of Coulomb's law of force between charges. Phys Rev. 1936;50:1066–71.
[26] Williams ER, Faller JE, Hill HA. New experimental test of Coulomb's law: A laboratory upper limit on the photon rest mass. Phys Rev Lett. 1971;26:721–4.
[27] Celozzi S, Araneo R, Lovat G. Electromagnetic shielding. Hoboken, New Jersey: John Wiley & Sons, Inc; 2008. p. 263–81.
[28] Rashba EI. Symmetry of energy bands in crystals of wurtzite type: I. symmetry of bands disregarding spin-orbit interaction. Sov Phys Solid State. 1959;1:368–80.
[29] Bychkov YA, Rashba EI. Properties of a 2D electron gas with lifted spectral degeneracy. JETP Lett. 1984;39:66–9.
[30] Stein D, Klitzing KV, Weimann G. Electron spin resonance on GaAs-AlxGa1-xAs heterostructures. Phys Rev Lett. 1983;51(2):130–3.
[31] Lüth H. Solid Surfaces, interfaces and thin films. 5th edn. Berlin: Springer Berlin Heidelberg; 2010. p. 263–76.
[32] Zhu LN, Xu BS, Wang HD, Wang CB. Effect of residual stress on the nanoindentation response of (100) copper single crystal, Mate. Chem Phys. 2012;136:561–5.
[33] Jang DY, Watkins TR, Kozaczek KJ, Hubbard CR, Cavin OB. Surface residual stresses in machined austenitic stainless steel. Wear. 1996;194:168–73.
[34] Shet C, Deng X. Residual stresses and strains in orthogonal metal cutting. Inter J Mach Tools Manuf. 2003;43:573–87.
[35] Garrett JL, Kim J, Munday JN. Measuring the effect of electrostatic patch potentials in Casimir force experiments. Phys Rev Res. 2020;2(023355):1–5.
[36] Damascelli A, Hussain Z, Zhi-Xun S. Angle-resolved photoemission studies of the cuprate superconductors. Rev Mod Phys. 2003;75(2):473–541.
[37] Pavarini E, Koch E, Brink J, van den, Sawatzky G, editors. Quantum materials: Experiments and theory modeling and simulation. Forschungszentrum Jülich. Vol. 6; 2016. p. 14.2.
[38] Harold JW, Zandvliet, Houselt AV. Scanning tunneling spectroscopy. Annu Rev Anal Chem. 2009;2:37–55.
[39] Tersoff J, Hamann DR. Theory of the scanning tunneling microscope. Phys Rev B. 1985;31(2):805–13.
[40] Vries RJD, Saedi A, Kockmann D, Houselt AV, Poelsema B, Zandvliet HJW. Spatial mapping of the inverse decay length using scanning tunneling microscopy. Appl Phys Lett. 2008;92(174101):1–3.
[41] Feenstra RM, Stroscio JA, Fein AP. Tunneling spectroscopy of the Si (111) 2 × 1 surface. Surf Sci. 1987;181:295–306.
[42] Huang YJ. Discovery of a new transport mechanism and physical origin of Hume-Rothery rules. 2021, viXra:1902.0264.
[43] Yan SH. Fundamentals of solid state physics. 3rd edn. Beijing: Beijing University Press; 2011. p. 1920188–9.
[44] Teorell T. Studies on the "diffusion effect" upon ionic distribution–I some theoretical considerations. Proc Natl Acad Sci U S A. 1935;21:152–61.
[45] Okamoto H, Schlesinger ME, Mueller EM. ASM Handbook Volume 3: Alloy phase diagrams. Russell, Ohio, USA: ASM International; 2016.
[46] Peng LX, Ringe E, Van Duyne RP, Marks LD. Segregation in bimetallic nanoparticles. Phys Chem Chem Phys. 2015;17:27940–51.
[47] Cui CH, Gan L, Heggen M, Rudi S, Strasser P. Compositional segregation in shaped Pt alloy nanoparticles and their structural behavior during electrocatalysis. Nat Mater. 2013;12:765–71.
[48] Chen C, Kang YJ, Huo ZY, Zhu ZW, Huang WY, Xin HL, et al. Highly crystalline multimetallic nanoframes with three-dimensional electrocatalytic surfaces. Science. 2014;343:1339–42.
[49] Wang KW, Chung SR, Liu CW. Surface segregation of PdxNi100-x alloy nanoparticles. J Phys Chem C. 2008;112:10242–6.

[50] Fowler RH, Nordheim L. Electron emission in intense electric fields, proceedings of the royal society of London. Proc R Soc Lond A, Contain Pap Math Phys Character. 1928;119(781):173–81.
[51] Huang WJ, Sun R, Tao J, Menard LD, Nuzzo RG, Zuo JM. Coordination-dependent surface atomic contraction in nanocrystals revealed by coherent diffraction. Nat Mater. 2008;7:308–13.
[52] Nunes AC, Lin D. Effects of surface relaxation on powder diffraction patterns of very fine particles. J Appl Cryst. 1995;28:274–8.
[53] Ishikawa K, Uemori T. Surface relaxation in ferroelectric perovskite. Phys Rev B. 1999;60(17):11841–5.
[54] Mays CW, Vermaak JS, Wilsdorf DK. On surface stress and surface tension: II. Determination of the surface stress of gold. Surf Sci. 1968;12:134–40.
[55] Solliard C, Flueli M. Surface stress and size effect on the lattice parameter in small particles of gold and platinum. Surf Sci. 1985;156:487–94.
[56] Jiang Q, Liang LH, Zhao DS. Lattice contraction and surface stress of fcc nanocrystals. J Phys Chem B. 2001;105(27):6275–7.
[57] Wolfer WG. Elastic properties of surfaces on nanoparticles. Acta Mater. 2011;59:7736–43.
[58] Huang YJ. Possible source of the earth's geomagnetic field. 2017, viXra: 1709.0024.
[59] Wang RM, Dmitrieva O, Farle M, Dumpich G, Ye HQ, Poppa H, et al. Layer resolved structural relaxation at the surface of magnetic FePt icosahedral nanoparticles. Phys Rev Lett. 2008;100(017205):1–4.
[60] Wang ZC. Thermodynamics statistical physics. 5th edn. Beijing: Higher Education Press; 2013. p. 89−93, 267−71.
[61] Lin ZH. Thermodynamics and statistical physics. 1st edn. Beijing: Peking University Press; 2007. p. 98.
[62] Wang ZP, Sun ZP, Jin M. Physical chemistry of surface. 1st edn. Shanghai: Tongji University Press; 2015. p. 172–3.
[63] Ghosh D, Chattopadhyay N. Gold and silver nanoparticle based superquenching of fluorescence: A review. J Lumin. 2015;160:223–32.
[64] Bhogale A, Patel N, Mariam J, Dongre PM, Miotello A, Kothari DC. Comprehensive studies on the interaction of copper nanoparticles with bovine serum albumin using various spectroscopies. Colloids Surf B Biointerfaces. 2014;113:276–84.
[65] Fleischmann M, Hendra PJ, McQuillan AJ. Raman spectra of pyridine adsorbed at a silver electrode. Chem Phys Lett. 1974;26:163–6.
[66] Jeanmaire DL, Van Duyne RP. Surface Raman spectroelectrochemistry. J Electroanal Chem Interfacial Electrochem. 1977;84:1–20.
[67] Albrecht MG, Creighton JA. Anomalously intense Raman spectra of pyridine at a silver electrode. J Am Chem Soc. 1977;99:5215–7.
[68] Ding SY, You EM, Tian ZQ, Moskovits M. Electromagnetic theories of surface-enhanced Raman spectroscopy. Chem Soc Rev. 2017;46:4042–76.
[69] Pilot R, Signorini R, Durante C, Orian L, Bhamidipati M, Fabris L. A Review on surface-enhanced Raman scattering. Biosensors. 2019;9(57):1–100.
[70] Langer J, De Aberasturi DJ, Aizpurua J, Ramon A, Puebla A, Auguié B, et al. Present and future of surface-enhanced Raman scattering. ACS Nano. 2020;14:28–117.
[71] Le Ru EC, Etchegoin PG. Principles of Surface Enhanced Raman Spectroscopy. Amsterdam, The Netherlands: Elsevier; 2009.
[72] Stiles PL, Dieringer JA, Shah NC, Van Duyne RP. Surface-enhanced Raman spectroscopy. Annu Rev Anal Chem. 2008;1:601–26.
[73] Milekhin AG, Sveshnikova LL, Duda TA, Yeryukov NA, Rodyakina EE, Gutakovskii AK, et al. Surface-enhanced Raman spectroscopy of semiconductor nanostructures. Phys E. 2016;75:210–22.
[74] Michieli N, Pilot R, Russo V, Scian C, Todescato F, Signorini R, et al. Oxidation effects on the SERS response of silver nanoprism arrays. RSC Adv. 2017;7:369–78.
[75] Wang XT, Shi WS, She GW, Mu LX. Surface-enhanced Raman scattering (SERS) on transition metal and semiconductor nanostructures. Phys Chem Chem Phys. 2012;14:5891–901.
[76] Gao Y, Gao N, Li HD, Yuan XX, Wang QL, Cheng SH, et al. Semiconductor SERS of diamond. Nanoscale. 2018;10:15788–92.
[77] Itoh T, Yamamoto YS. Reproduction of surface-enhanced resonant Raman scattering and fluorescence spectra of a strong coupling system composed of a single silver nanoparticle dimer and a few dye molecules. J Chem Phys. 2018;149(244701):1–11.
[78] Yoshida KI, Itoh T, Tamaru H, Biju V, Ishikawa M, Oza Y. Quantitative evaluation of electromagnetic enhancement in surface-enhanced resonance Raman scattering from plasmonic properties and morphologies of individual Ag nanostructures. Phys Rev B. 2010;81(115406):1–9.
[79] Le Ru EC. Etchegoin PG, Principles of Surface-enhanced Raman spectroscopy and related plasmonic effects. 1st edn. Oxford, UK: Elsevier B. V; 2009.
[80] Li JF, Huang YF, Ding Y, Yang ZL, Li SB, Zhou XS, et al. Shell-isolated nanoparticle-enhanced Raman spectroscopy. Nature. 2010;464:392–5.
[81] Li JF, Zhang YJ, Ding SY, Panneerselvam R, Tian ZQ. Core−shell nanoparticle-enhanced Raman spectroscopy. Chem Rev. 2017;117(7):5002–69.
[82] Benz F, Schmidt MK, Dreismann A, Chikkaraddy R, Zhang Y, Demetriadou A, et al. Single-molecule optomechanics in picocavities. Science. 2016;354(6313):726–9.
[83] Shin HH, Yeon GJ, Choi HK, Park SM, Lee KS, Kim ZH. Frequency-domain proof of the existence of atomic-scale SERS hot-spots. Nano Lett. 2018;18:262–71.
[84] Moskovits M, DiLella DP, Maynard KJ. Surface Raman spectroscopy of a number of cyclic and molecular reorientation aromatic molecules adsorbed on silver: selection rules. Langmuir. 1988;4(1):61–76.
[85] Kneipp K, Moskovits M, Kneipp H, editors. Surface-enhanced Raman scattering-physics and applications. Top Appl Phys. 2006;103:125–46.
[86] Huang QJ, Li XQ, Yao JL, Ren B, Cai WB, Gao JS, et al. Extending surface Raman spectroscopic studies to transition metals for practical applications III. effects of surface roughening procedure on surface-enhanced Raman spectroscopy from nickel and platinum electrodes. Surf Sci. 1999;427–428:162–6.
[87] Cai WB, Ren B, Li XQ, She CX, Liu FM, Cai XW, et al. Investigation of surface-enhanced Raman scattering from platinum electrodes using a confocal Raman microscope: dependence of surface roughening pretreatment. Surf Sci. 1998;406:9–22.
[88] Cao PG, Yao JL, Ren B, Mao BW, Gu RA, Tian ZQ. Surface-enhanced Raman scattering from bare Fe electrode surfaces. Chem Phys Lett. 2000;316:1–5.
[89] Batra RC, Porfiri M, Spinello D. Review of modeling electrostatically actuated microelectromechanical systems. Smart Mater Struct. 2007;16:R23–31.

[90] Zhang WM, Meng G, Chen D. Stability, nonlinearity and reliability of electrostatically actuated MEMS devices. Sensors. 2007;7:760–96.
[91] Zhang WM, Yan H, Peng ZK, Meng G. Electrostatic pull-in instability in MEMS/NEMS: a review. Sens Actuators A Phys. 2014;214:187–214. doi: 10.1016/j.sna.2014.04.025.
[92] Pamidighantam S, Puers R, Baert K, Tilmans HAC. Pull-in voltage analysis of electrostatically actuated beam structures with fixed-fixed and fixed-free end conditions. J Micromech Microeng. 2002;12:458–64.
[93] Versaci M, Jannelli A, Morabito FC, Angiulli G. A semi-linear elliptic model for a circular membrane MEMS device considering the effect of the fringing field. Sensor. 2021;21(5237):1–27. doi: 10.3390/s21155237.
[94] Liu ZW, Lou XH, Gao JX. Deformation analysis of MEMS structures by modified digital moiré methods. Opt Lasers Eng. 2010;48:1067–75.
[95] Joo JW, Choa SH. Deformation behavior of MEMS gyroscope sensor package subjected to temperature change. IEEE Trans Compon Packag Technol. 2007;30:346–54.
[96] Peirs J, Reynaerts D, Brussel HV. Scale effects and thermal considerations for micro-actuators. Proceedings of the 1998 IEEE International Conference on Robotics & Automation. Leuven, Belgium: 1998. p. 1516–21.
[97] Hohlfeld RG, Cohen N. Self-similarity and the geometric requirements for frequency independence in antennae. Fractals. 1999;7:79–84.
[98] Werner DH, Ganguly S. An overview of fractal antenna engineering research. IEEE Antennas Propag Mag. 2003;459(1):38–57.
[99] Krzysztofik WJ. Fractal geometry in electromagnetic applications from antenna to metamaterials. Microw Rev. 2013;19:3–14.
[100] Krzysztofik WJ. Fractals in antennas and metamaterials applications. London, UK: InTechOpen; 2017. doi: 10.5772/intechopen.68188.
[101] Guariglia E. Entropy and fractal antennas. Entropy. 2016;18(84):1–17.
[102] Guariglia E. Harmonic sierpinski gasket and applications. Entropy. 2018;20(714):1–12.
[103] Mahdy AMS, Lotfy K, Ahmed MH, Bary AE. Electromagnetic Hall current effect and fractional heat order for microtemperature photo-excited semiconductor medium with laser pulses. Res Phys. 2020;17(103161):1–9. doi: 10.1016/j.rinp.2020.103161.
[104] Mahdy AMS, Lotfy K, Ismail EA, Bary AE, Ahmed M, Dahdouh AAE, Analytical solutions of time-fractional heat order for a magneto-photothermal semiconductor medium with Thomson effects and initial stress, Res Phys, 2020;18:(103174):1–11.